Agenzia Nazionale per le Nuove Tecnologie,
l'Energia e lo Sviluppo Economico Sostenibile

Ministero dello Sviluppo Economico

RICERCA DI SISTEMA ELETTRICO

CERSE-UNIPI RL 1077/2010

CFD Analysis in support to the experimental activity on the mixing processes in the downcomer and lower plenum of IRIS reactor

A. Carnevali, N. Forgione, G. Galgani, F. Oriolo

Report RdS/2010/75

CFD ANALYSIS IN SUPPORT TO THE EXPERIMENTAL ACTIVITY ON THE MIXING PROCESSES IN THE DOWNCOMER AND LOWER PLENUM OF IRIS REACTOR

A. Carnevali, N. Forgione, G. Galgani, F. Oriolo

Settembre 2010

Report Ricerca di Sistema Elettrico
Accordo di Programma Ministero dello Sviluppo Economico – ENEA
Area: Produzione e fonti energetiche
Tema: Nuovo Nucleare da Fissione

Responsabile Tema: Stefano Monti, ENEA

CIRTEN

CONSORZIO INTERUNIVERSITARIO

PER LA RICERCA TECNOLOGICA NUCLEARE

UNIVERSITA' DI PISA

DIPARTIMENTO DI INGEGNERIA MECCANICA, NUCLEARE E DELLA PRODUZIONE

CFD analysis in support to the experimental activity on the mixing processes in the downcomer and lower plenum of IRIS reactor

CIRTEN - UNIPI RL 1077/2010

AUTORI

A.Carnevali, N. Forgione, G. Galgani, F. Oriolo

Pisa, August 2010

Lavoro svolto in esecuzione della linea progettuale LP2 punto F - AdP ENEA MSE del 21/06/07 Tema 5.2.5.8 – "Nuovo Nucleare da Fissione".

ABSTRACT

The present work represents a contribution to the design of an experimental facility planned to provide data relevant for the mixing phenomena in the downcomer and lower plenum of the IRIS reactor when a DVI line break accident (SBLOCA) occurs and for CFD codes validation.

In particular, in order to evaluate the boron concentration in the reactor core inlet, when different mass flow rates coming from DVI lines and steam generators (characterized by different boron concentration) mix, a facility, scaled 1:5 respect to the IRIS reactor, has been proposed and designed by the University of Pisa. The thermal-hydraulic behaviour of the facility has been simulated by using the FLUENT code. The boundary conditions related to the postulated accident scenarios to be used in the CFD calculations were drawn from previous information coming from system code simulations.

After a description of the scaling analysis approach, a qualitative value of temperature distribution in the core inlet will be shown and discussed for several cases, considering three different time windows after accident (600, 20000 and 60000 s). Furthermore, the importance of the scaling analysis methodology assumptions will be discussed, and their consequences will be shown. Beside, four different DVI lengths have been considered in order to figure out how their penetration in the down comer can improve the uniformity of the boron concentration at the core inlet.

The present report includes both the foreseen activities LP2. F1 and LP2.F2 for a better understanding of the treated scientific issues.

INDEX

1. FACILITY AND SCALING ANALYSIS

1.1 Facility description

The optically transparent separate-effect facility [1,2] consists of a 1:5 scaled model of the downcomer and of the lower plenum of IRIS, designed with a particular care to represent the geometrical configuration of the real plant (see red marked zone in fig. 1.1). The geometrical similarity between the model and the original reactor is respected until the core inlet, which is not reproduced in the facility and which is then excluded from the similarity [5].

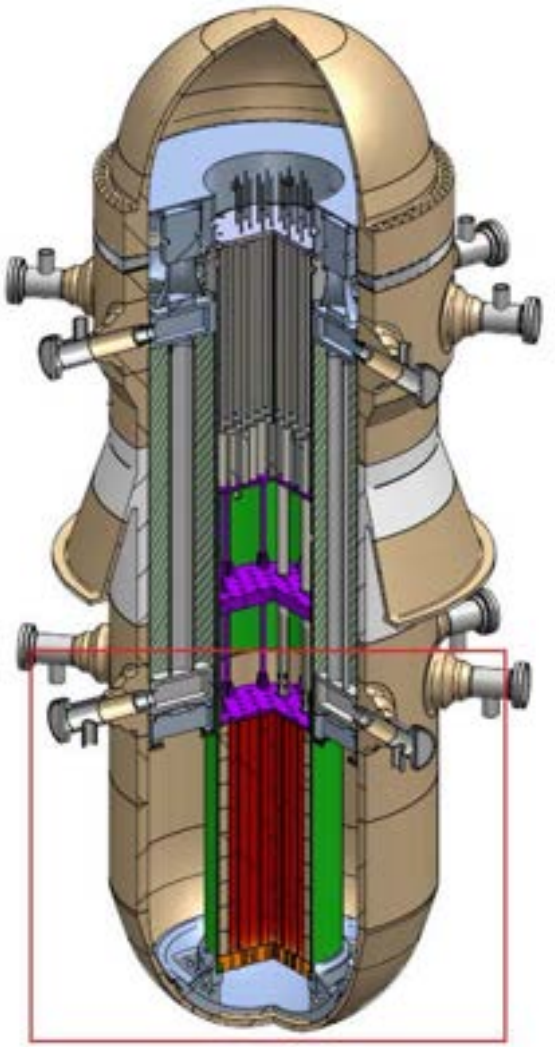

Figure 1.1. IRIS reactor (with the marked downcomer and the lower plenum region).

The facility is composed by a lower hemispherical shell of Plexiglas® having a radius of 0.623 m and representing the lower downcomer, connected to a cylindrical wall in Plexiglas® having the same radius of the shell and a length of 0.804 m, as is represented in fig. 1.2, fig. 1.3 and in fig. 1.4. The downcomer region is completed by an internal stainless steel cylinder having an external radius of 0.285 m, longer respect to the external cylinder. In the upper part of the facility, eight conical stainless steel pipes simulate the eight downcomer mass flow inlets coming from the eight IRIS steam generators (not reproduced in the facility). The steam generator inlets have been located at 22.5° angle between each other. Two stainless steel tubes, representing the two DVIs of the IRIS reactor, are also considered, with a nominal length of 0.804 m and an internal diameter of 0.0158 m. Moreover, the length of the two DVI pipes inside the downcomer can be changed to analyse the effects of their penetration inside the vessel.

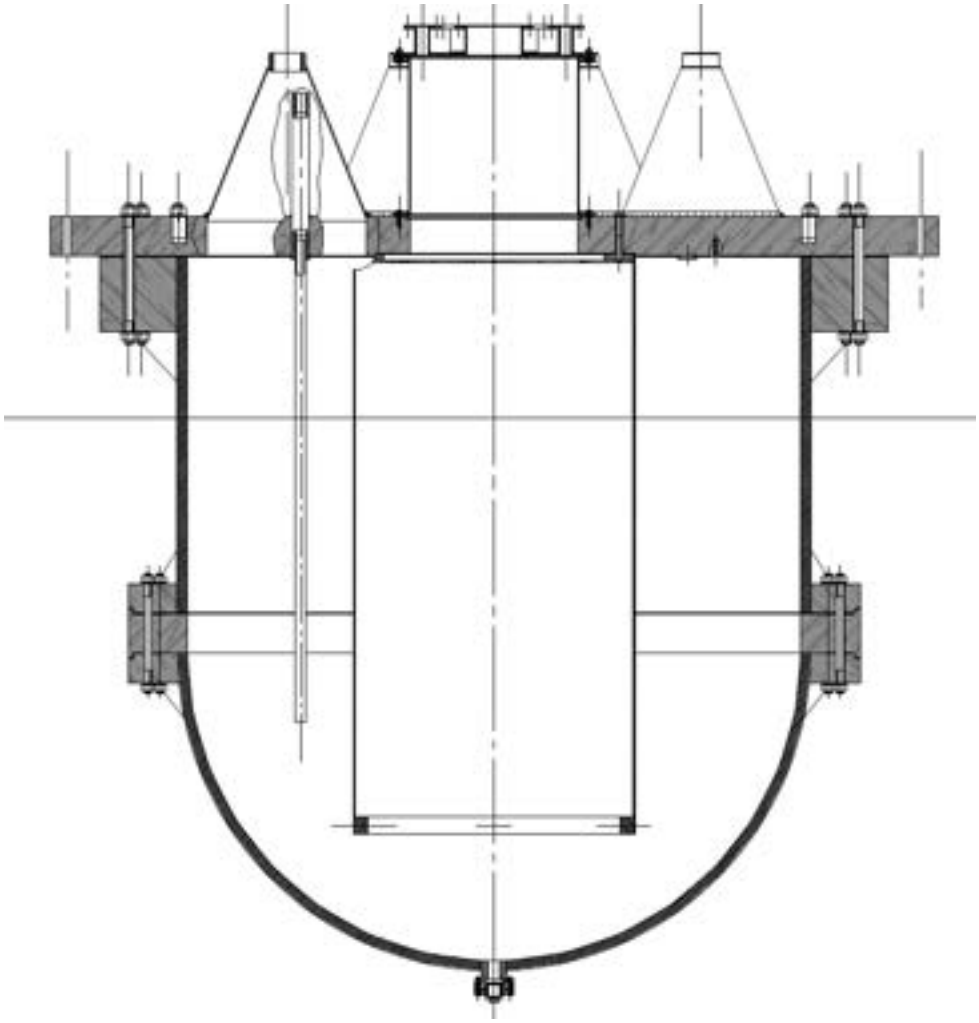

Figure 1.2. Experimental facility: longitudinal cross section.

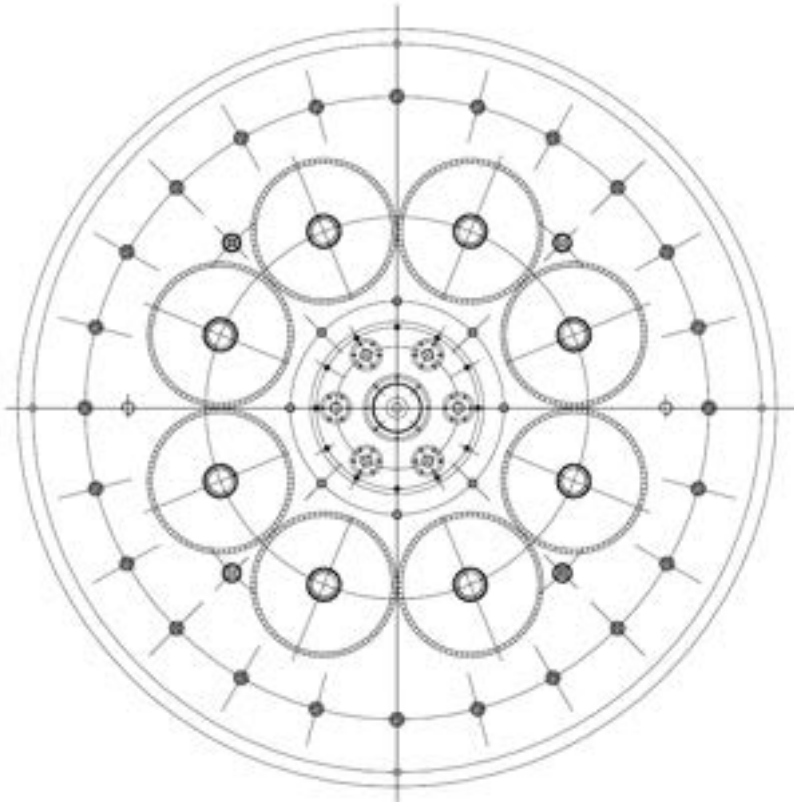

Figure 1.3. Experimental facility: upper view
(it is possible to see the eight mass flow inlet and the singular central outlet).

The stainless steel flange which links the external cylinder and the hemispherical shell (see the red arrows in fig. 1.4) is provided with 24 radial holes, which can be used to introduce pressure and temperature sensors in the facility. The outlet flange in the upper part of the facility, which discharges the water from the facility to the drainage after its run through the test section, is also equipped with six holes which allow to perform intrusive measurements in the internal stainless steel cylinder, as represented in fig. 1.5.

The facility is conceived to be flexible enough to make feasible both internal measurements (thermocouples and RTDs for the boron concentration, hot-wire anemomentry for investigating velocity and flow detailed structures, pressure and flow rate sensors) and non-intrusive measurements. In particular, the use of Plexiglas® for the external cylinder and for the hemispherical shell makes the facility suitable for the use of flow visualization systems, like Video Images Recorded with high speed resolution, Laser Doppler Anemometry, Particle Image Velocimetry and Laser Induced Fluorescence [6].

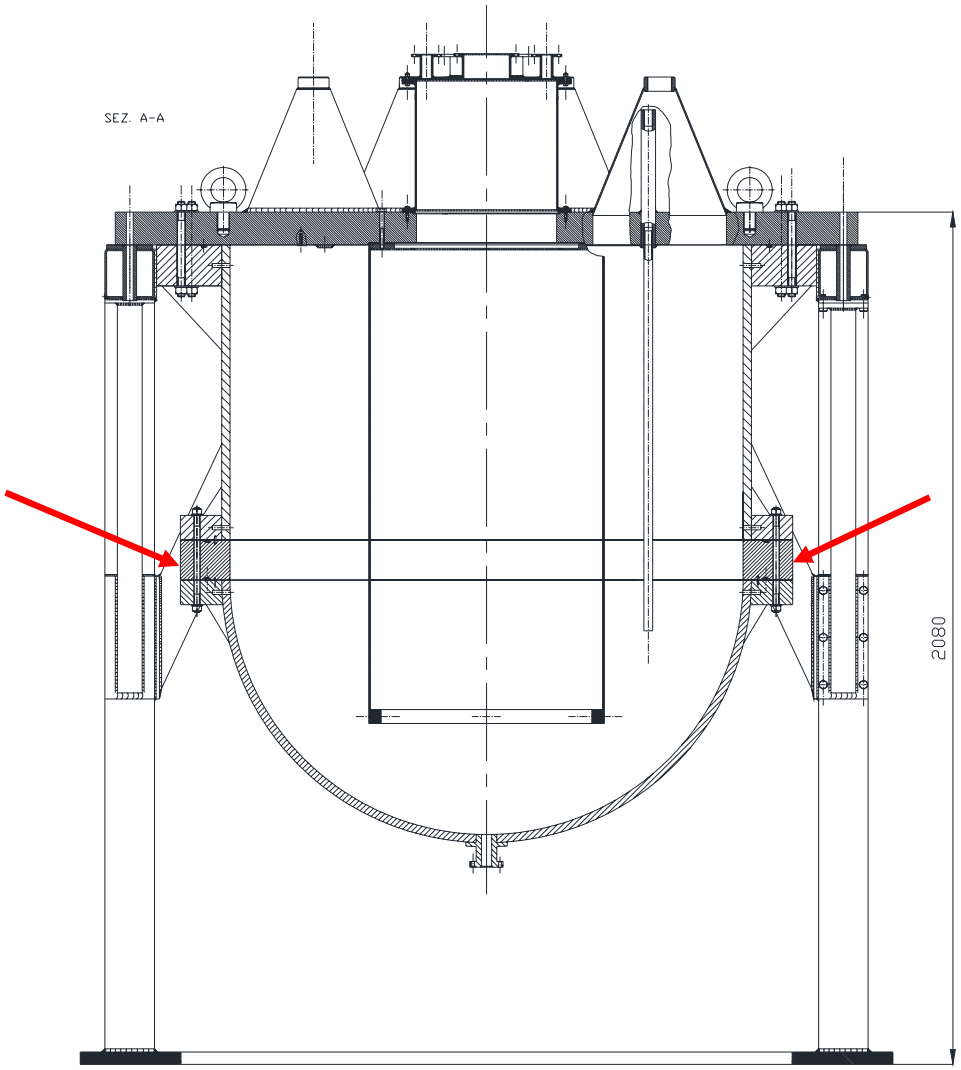

Figure 1.4. Experimental facility: cross section with external supports.

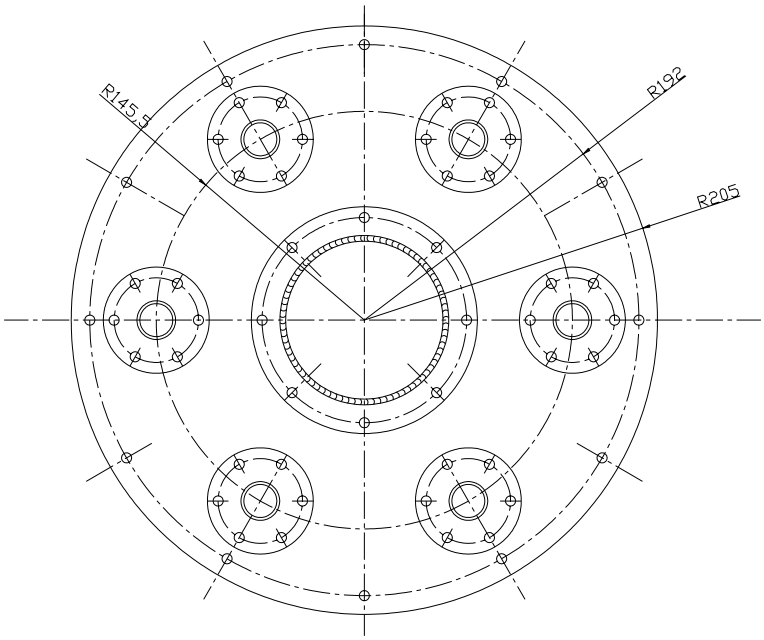

Figure 1.5. Experimental facility: holes for the measurements systems, around the upper outlet.

1.2 Scaling approaches

Since the large size of IRIS, the relative Reynolds numbers assume high values in the reactor downcomer; it means that turbulent mixing is more important than molecular diffusion. So, when a velocity field is assumed, mass and heat transfer behaviour are similar. Hence, a perturbation of the boron concentration can be studied starting from the perturbation of the temperature field, once buoyancy effects are negligible. As it can be noted, with some simplifications, the boron concentration equation appears formally similar to the energy equation:

$$\frac{\partial(\rho T)}{\partial t} + w_i \cdot \frac{\partial(\rho T)}{\partial x_i} = \frac{\partial}{\partial x_i}\left(D_{T,t} \frac{\partial(\rho T)}{\partial x_i} \right)$$

$$\frac{\partial(\rho c_B)}{\partial t} + w_i \cdot \frac{\partial(\rho c_B)}{\partial x_i} = \frac{\partial}{\partial x_i}\left(D_{C,t} \frac{\partial(\rho c_B)}{\partial x_i} \right)$$

where T is the fluid temperature, c_B is boron concentration, $D_{T,t}$ is the turbulent diffusivity coefficient for the temperature and $D_{c,t}$ is the turbulent diffusivity coefficient referred to the boron concentration. Hence, the temperature and the boron concentration profiles become similar once both the turbulent diffusivity coefficients assume values of the same order of magnitude [3].

Based on this hypothesis, the temperature field related to the mixing processes in IRIS and in the facility downcomer has been investigated. Starting from RELAP simulation data [4] of a DVI line break in IRIS, four time temporal scenarios have been studied in detail. It has been analysed the *nominal* case of work and t = 600 s, t = 20000 s and t = 60000 s after the DVI line break event. For all these cases, mass flow rates, temperatures and pressures have been identified and are listed in table 1.1.

	NOMINAL	INC-600s	INC-20000s	INC-60000s
DC flow rate				
Mass flow rate [kg/s]	4711.98	496.329	110.288	350.146
Temperature [K]	565	516.944	404.058	405.301
Pressure [MPa]	15.5	3.59	0.363	0.313
DVI intact flow rate				
Mass flow rate [kg/s]	-	5.8391	2.47	0.916
Temperature [K]	-	343.534	337.6	389.62
Pressure [MPa]	-	3.62	0.41	0.36
DVI break flow rate				
Mass flow rate [kg/s]	-	-13.4554	-0.431	2.456
Temperature [K]	-	517.127	402.775	401.416
Pressure [MPa]	-	3.54	0.41	0.36

Table 1.1. Main IRIS variables for different time events.

Since the fluid-dynamics of the mixing processes which occurs in the IRIS downcomer is difficult to analyse and to reproduce with a scaled facility, the idea is to adopt some different criteria for the facility design which allow to maintain some of the most influent parameters of larger affect on the relevant mixing phenomena, equal to that observed in IRIS. In this work, in order to evaluate the mass flow rates through the facility, two different scaling criteria have been adopted:

1) constant residence time approach, by maintaining a constant residence time;
2) constant velocity approach, by keeping the same fluid average velocity as in IRIS.

Since we are interested in turbulent flows, it should be interesting to keep the same Reynolds number as in IRIS, but due to the reduced facility dimension, this should be possible only with a much higher value of the flow velocity than that observed in IRIS and this value is too high to be adopted for the experimental measurements on the facility. Hereinafter the general procedures [4] in order to evaluate the facility mass flow rate through the inlets are reported, by keeping the same residence time and the same average velocity, respectively.

Maintaining the same residence time we obtain:

$$\frac{(\tau)_{IRIS}}{(\tau)_{\exp}} = \frac{(L/w)_{IRIS}}{(L/w)_{\exp}} = \frac{(L)_{IRIS}}{(L)_{\exp}} \cdot \frac{(w)_{\exp}}{(w)_{IRIS}} = 1 \;\Rightarrow\; (w)_{\exp} = \frac{(L)_{\exp}}{(L)_{IRIS}} \cdot (w)_{IRIS} = \frac{1}{5} \cdot (w)_{IRIS}$$

$$\left[\dot{m}_{\exp}\right]_{\tau} = \rho_{\exp} \cdot w_{\exp} \cdot A_{\exp}$$

while maintaining the same velocity we obtain

$$w_{IRIS} = w_{\exp} \quad \Rightarrow \quad \frac{\dot{m}_{IRIS}}{\rho_{IRIS} \cdot A_{IRIS}} = \frac{\dot{m}_{\exp}}{\rho_{\exp} \cdot A_{\exp}}$$

$$\left[\dot{m}_{\exp}\right]_w = \frac{\dot{m}_{IRIS}}{\rho_{IRIS}} \cdot \frac{\rho_{\exp}}{25}$$

Concerning with the temperature values assigned as boundary conditions, to perform the computational simulation of the mixing processes with the FLUENT code, it has been decided to adopt a temperature of T = 293.15 K (20°C) as values for the mass flow rates coming from the eight inlets to the downcomer; a higher temperature value of T = 343.15 K (70°C) has been set for the mass flow rates coming through the DVI lines.
It must be noted that in the facility the temperature differences between the DVI lines and the downcomer are assumed to be reversed with respect to IRIS for reasons of practical feasibility.
In the following tables, the general boundary conditions are shown for both the scaling criteria, for the different times considered after the DVI line break (i.e. *nominal*, t = 600 s, t = 20000 s and t = 60000 s).

	NOMINAL	INC-600s	INC-20000s	INC-60000s
DC flow rate				
Residence time criteria				
Mass flow rate [kg/s]	50.321	4.912	0.945	3.003
Temperature [K]	293.15	293.15	293.15	293.15
Pressure [MPa]	0.1	0.1	0.1	0.1
Velocity criteria				
Mass flow rate [kg/s]	253.503	24.559	4.725	15.014
Temperature [K]	293.15	293.15	293.15	293.15
Pressure [MPa]	0.1	0.1	0.1	0.1
DVI intact flow rate				
Residence time criteria				
Mass flow rate [kg/s]		0.048	0.020	0.008
Temperature [K]		343.15	343.15	343.15
Pressure [MPa]		0.1	0.1	0.1
Velocity criteria				
Mass flow rate [kg/s]		0.238	0.101	0.039
Temperature [K]		343.15	343.15	343.15
Pressure [MPa]		0.1	0.1	0.1
DVI break flow rate				
Residence time criteria				
Mass flow rate [kg/s]		-0.133	-0.004	0.0211
Temperature [K]		343.15	343.15	343.15
Pressure [MPa]		0.1	0.1	0.1
Velocity criteria				
Mass flow rate [kg/s]		-0.666	-0.018	0.105
Temperature [K]		343.15	343.15	343.15
Pressure [MPa]		0.1	0.1	0.1

Table 1.2. Boundary condition data for different time events,
achieved by using two different scaling approaches.

2. FLUENT simulations

2.1 Geometrical domains for IRIS and for the facility

The main differences between the geometries of IRIS and of the experimental facility regards the lower part of the volume representing the reactor core: in IRIS a perforated plate is present at the core inlet (see fig. 2.1), while a free surface has been considered for the facility. Furthermore, the plate used for the IRIS model has been reproduced in two configurations, both with and without core supports.

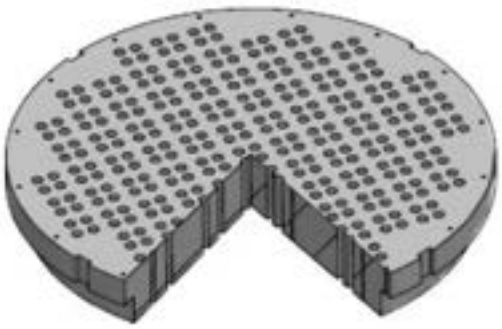

Figure 2.1. Lower perforated plate in IRIS core inlet.

The geometry obtained for IRIS is shown in fig. 2.2 and in fig. 2.3. It must be noted that, because of symmetry, only half facility and half reactor have been considered.

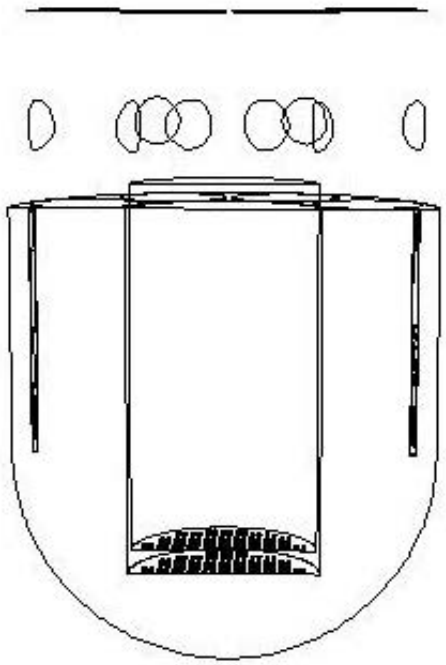

Figure 2.2. IRIS geometry without core supports.

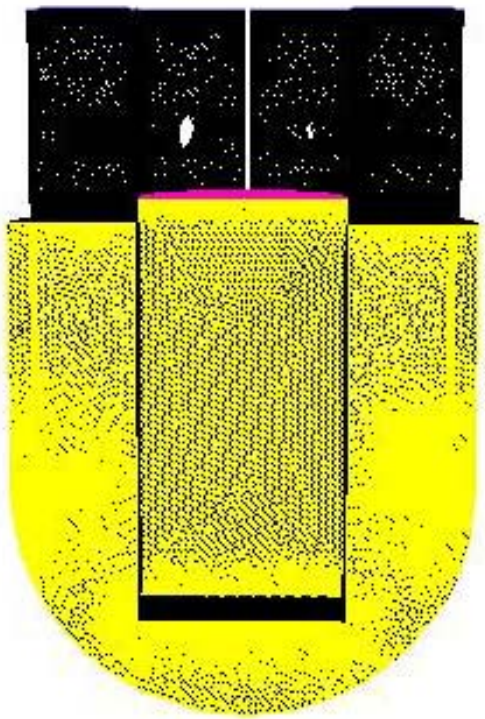

Figure 2.3. IRIS meshed geometry without core supports.

The model shown in fig. 2.2 is referred to the simpler one, which does not include the core supports. In fig. 2.4 it is reported a particular of the core inlet.

One of the goal of this work is to study how these components affect the mixing phenomena in IRIS and how the results could, eventually, suggest some improvement for the facility design and could support the definition of the possible experimental test conditions.

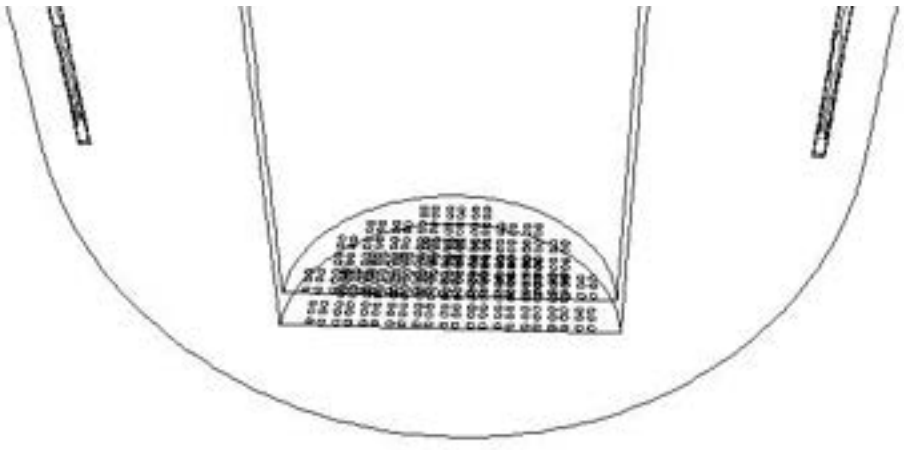

Figure 2.4. IRIS core inlet without supports.

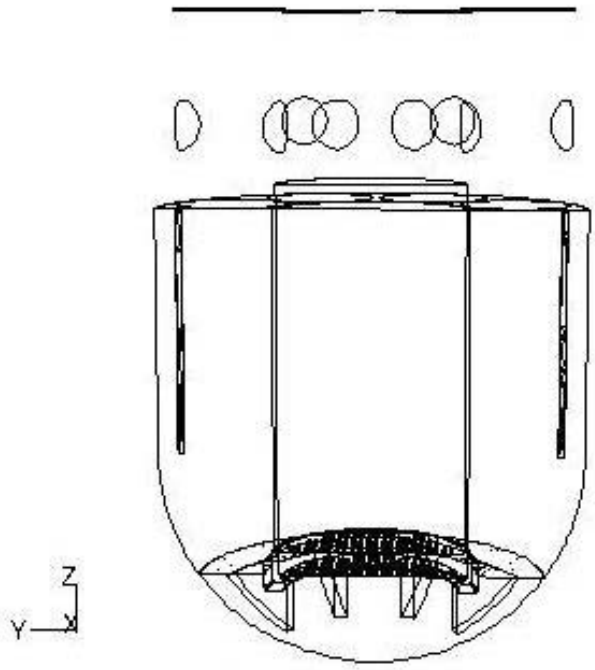

Figure 2.5. IRIS geometry with core supports.

The other IRIS configuration takes into account also the core supports at the core inlet, as it can be seen in fig. 2.5. The meshed model is reported in fig. 2.6. A particular of the supports used is shown in fig. 2.7: these supports consists of eight plates which are necessary to sustain the core in the right position inside the reactor vessel.

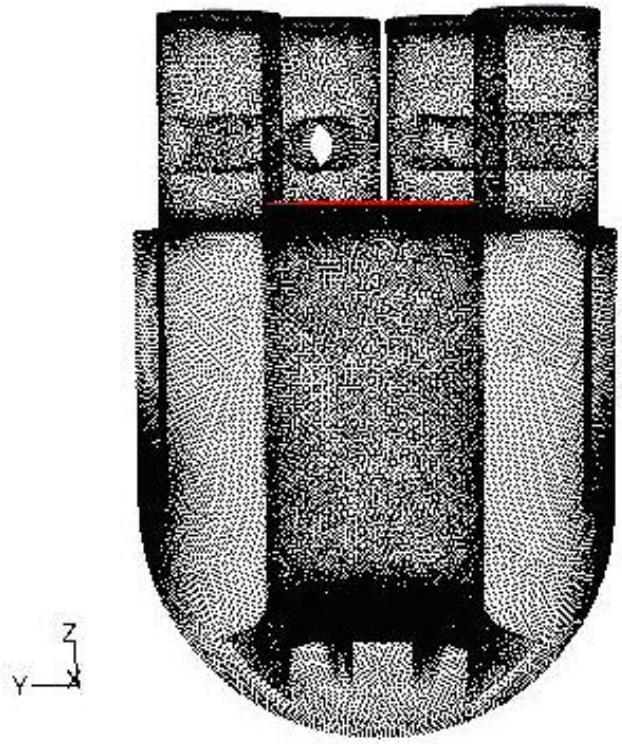

Figure 2.6. IRIS meshed geometry with core supports.

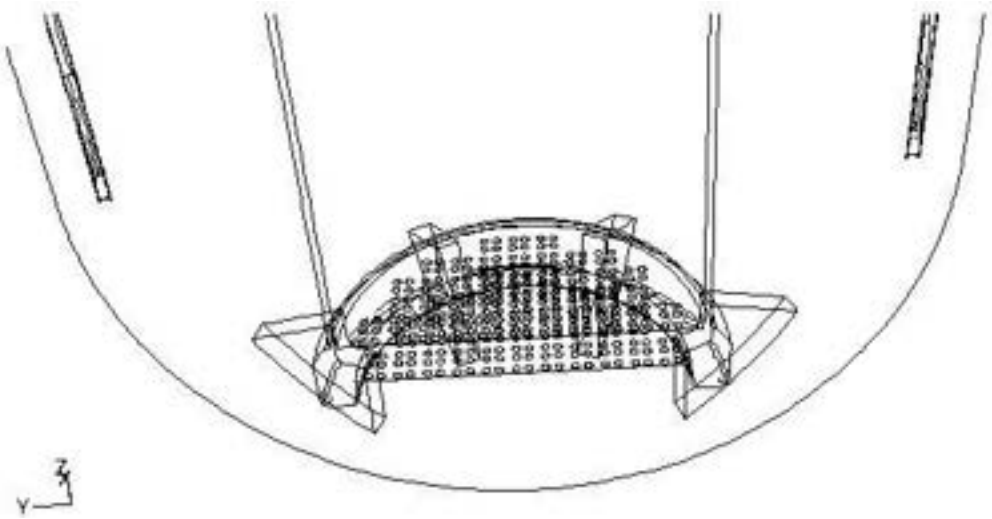

Figure 2.7. IRIS core inlet with supports.

Once examined both of the IRIS configurations, it is important to investigate the facility model implementation, as shown in fig. 2.8, fig. 2.9 and fig. 2.10. The general overview on the facility model is given in fig. 2.8, while in fig. 2.9 is presented the mesh used to discretize the volume of the downcomer. Moreover in fig. 2.10 it is shown the core inlet region: as already mentioned, this facility is similar to the IRIS reactor, except for the presence of the perforated plate at the bottom of the core inlet, which is not reproduced in the facility design.

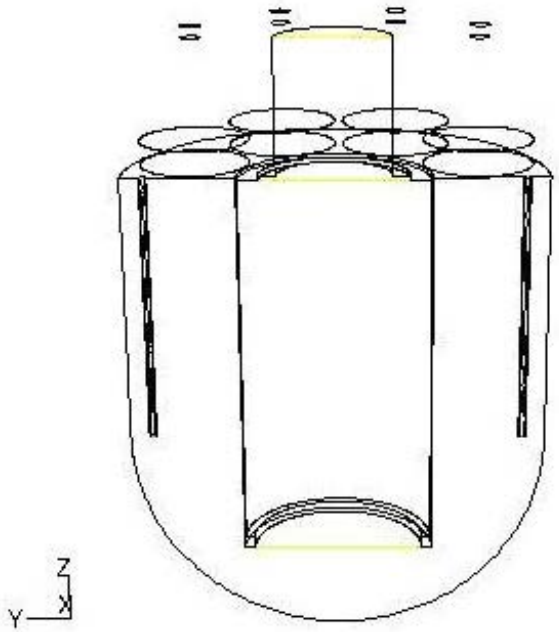

Figure 2.8. Facility geometry.

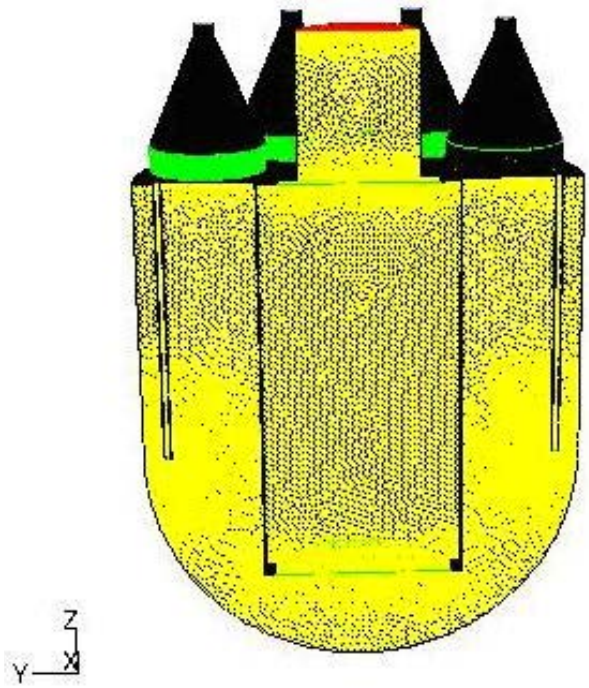

Figure 2.9. Facility meshed geometry.

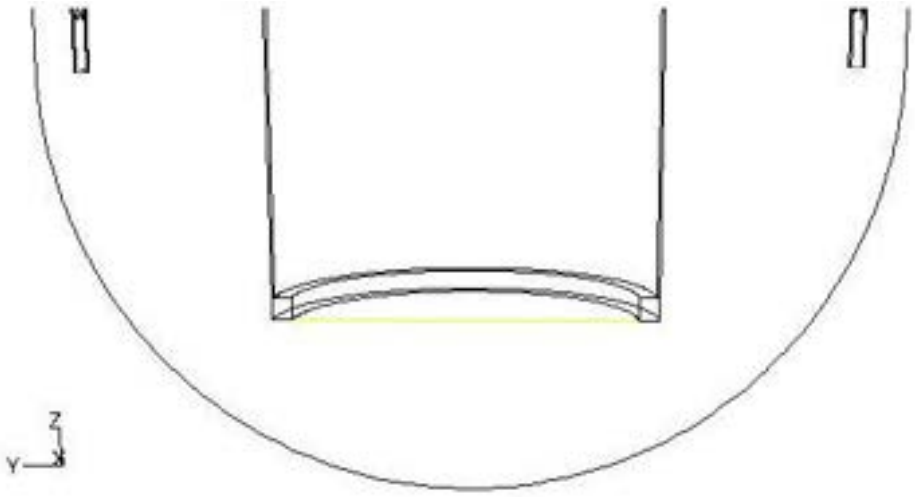

Figure 2.10. Enlargement of the facility domain in the “core inlet” region.

In a second phase, an appropriate porous region is foreseen to be collocated at the core inlet of the experimental facility, e.g. an honeycomb structure, to reproduce the effect of the lower perforated plate present in the IRIS core inlet.

Both for IRIS and for the facility, several size functions have been imposed during the meshing operations in all those parts characterized by a more difficult geometry and interested by complex fluid-dynamics phenomena; in particular, the use of the size function has been required to mesh and to discretize those zones which are closer to the core inlet, i.e. where different fluxes mix. In the following table 2.1, the number of the

cells adopted for the IRIS domains and for the facility domain are listed. Both for IRIS and for the facility a polyhedral mesh has been used to discretize the geometrical domain.

IRIS without supports	IRIS with supports	Facility
5'808'290 cells	5'644'003 cells	4'673'930 cells

Table 2.1. Number of cells used to mesh the IRIS domain (with and without supports) and the facility domain.

2.2 Operative and boundary conditions

The turbulence effects in all the simulations performed have been evaluated by the standard k-ε model.

Both in IRIS and in the facility, the geometry of the core has not been evaluated (except for the lower perforated plate at the core inlet for the IRIS model). The IRIS core consists in 264 nuclear fuel rods, placed in a 17 x 17 grid; so a strong pressure drop is expected in the crossing of the core itself. In order to avoid the difficulty to discretize and to model all the fuel rods and to safe computational time, a porosity region has been considered instead of the IRIS real core geometry to simulate the pressure drop along the core itself. This porosity region has been placed at the core inlet.

FLUENT software allows the user to follow several ways to consider a porosity region and for this case, it has been picked the 'Deriving Porous Media Inputs Based on Superficial Velocity, Using a Known Pressure Loss' option.

It consists on an evaluation of the inertial loss factor, as follows:

$$C_2 = \frac{K'_L}{thickness}$$

with

$$K'_L = K_L \cdot \frac{v^2_{A\%open}}{v^2_{100\%open}}$$

where *K* is the loss factor, while *A* indicates the ratio between the free flow area and the total area.

For the IRIS core, an indicative value of 10 has been assumed as *K*, and a 0.6 porosity fraction has been assumed by considering the plate shown in fig. 2.11 and in fig. 2.12.

Concerning the IRIS geometrical parameters for the fuel rods, a ratio *p*/*d* = 1.4 and an external diameter of *d* = 9.5 mm has been considered.

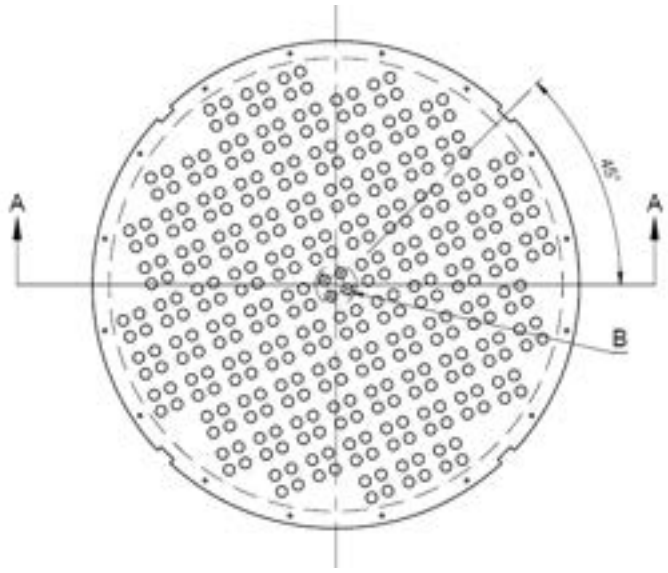

Figure 2.11. Perforated lower core plate for IRIS.

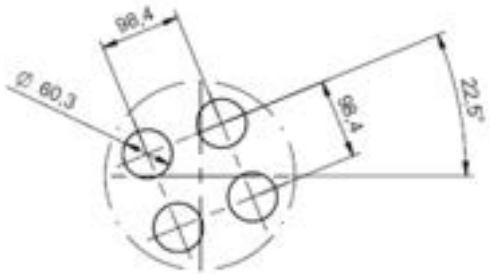

Figure 2.12. Holes geometrical data.

The effect of this imposed porosity region is shown in fig. 2.13. The trend of the static pressure in the IRIS reactor has been plotted referred to the nominal case. It can be noted that the static pressure is relatively high in the lower zone of the IRIS downcomer and it gradually reduces when the *z* coordinate grow up.

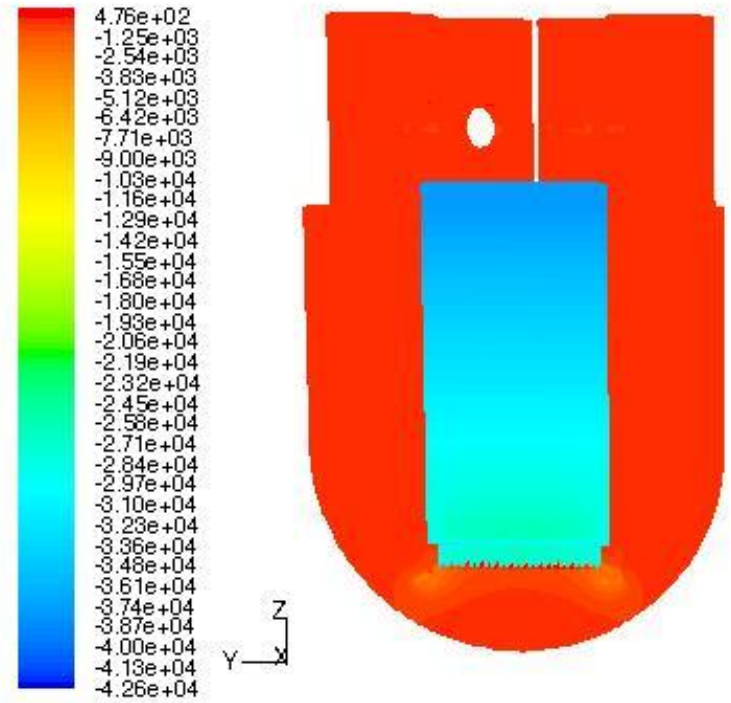

Figure 2.13. Static pressure distribution for the IRIS domain (nominal case).

A particular of the pressure trend exposed above at the core inlet is reported in fig. 2.14

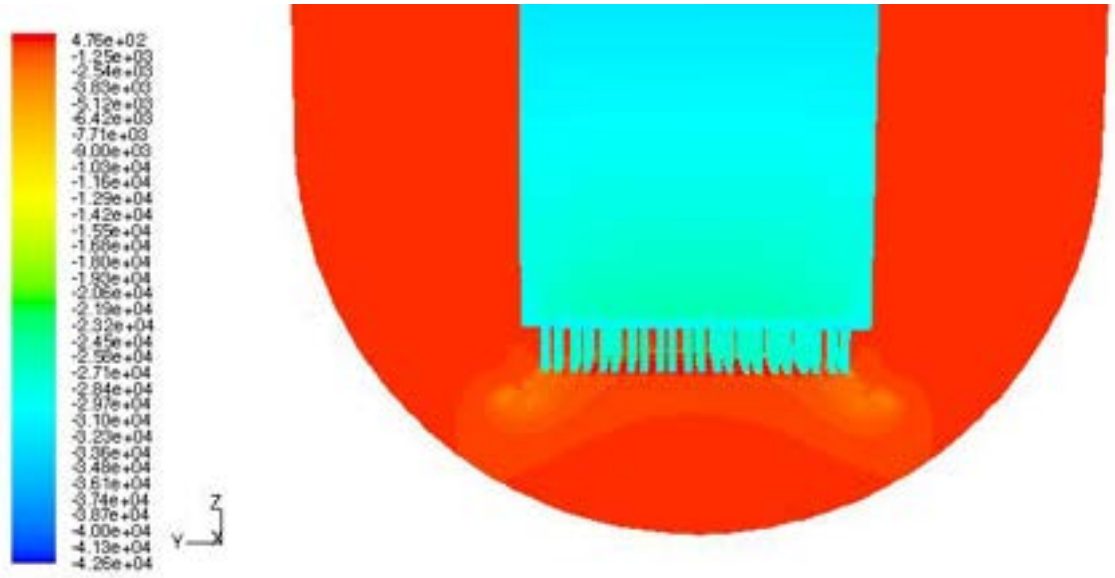

Figure 2.14. Static pressure distribution for the IRIS domain near the core inlet region.

It has been observed that, due to the lower mass flow rate of water entering in the experimental facility than that observed for the IRIS reactor and due to the conical shape of the mass flow inlets, the flow coming from the SGs does not show an homogeneous velocity profile: the mass flow distribution through the SGs has a velocity profile in the *z* direction which strongly depends to the plane coordinate. This effect causes a different mass flow distribution coming into the facility, and it should seriously affect the whole facility simulation results, because of a non constant velocity value entering the facility.

In order to explain the problem, vector velocity profiles referred to the facility case for nominal boundary conditions are shown in fig. 2.15 (porous region not present). The light blue arrows are observed in the upper part of the inlets for each SG and show a fluid velocity which is higher than that recorded in the lower part of the SGs, marked with dark blue arrows. Moreover, the velocity vectors show circular paths in the lower part of the inlets and the water flow rate seems to not cover homogeneously the whole inlet section.

In order to avoid this problem, some grids have been considered for the facility placed in the lower part of each SG inlet, to get an as much as possible homogeneous inlet flow rate to the downcomer. These grids have been simulated in the computational model by considering a porosity region, obtained in the same way of that previously explained

above. In this case the porosity has been assumed equal to 0.8 and a loss factor equal to 1.5 has been imposed.

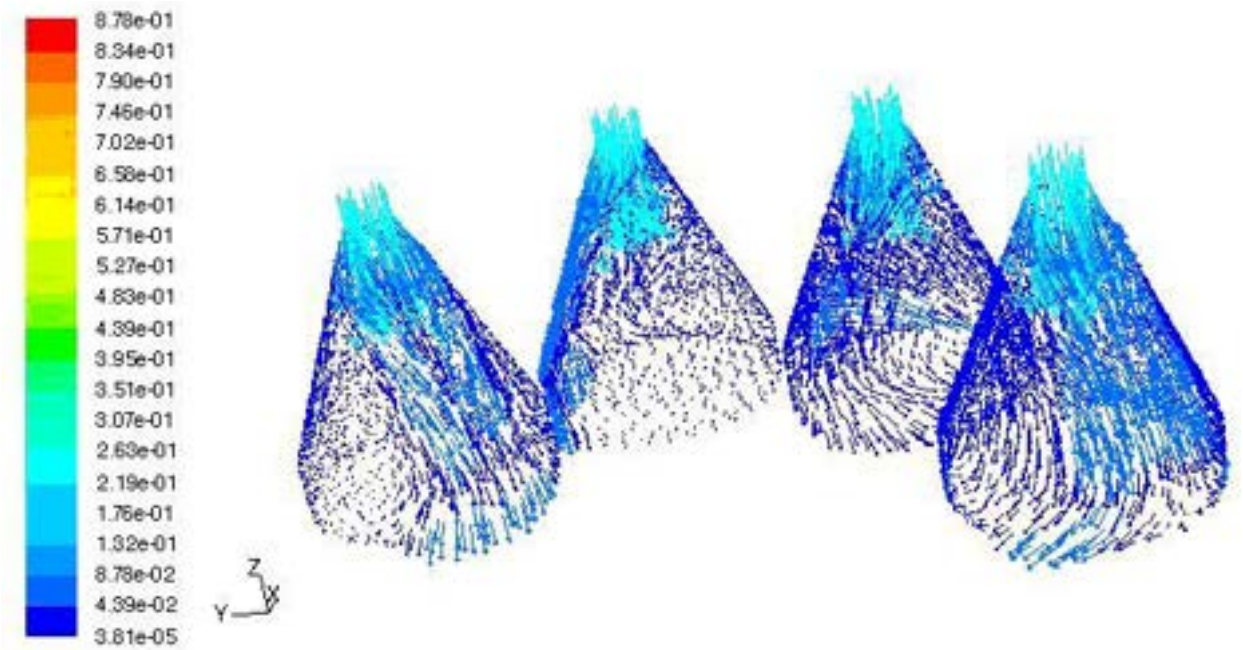

Figure 2.15. Velocity vector distribution in the inlet regions of the facility (nominal case).

The contour plots of the velocity along the *z* coordinate (normal to the transverse section) are plotted in the figures from 2.16 to 2.23 to analyse the effect of the introduction of these grids; the cross section of the facility chosen in these figures is referred to the zone immediately below the SGs. The *z*-velocity distribution has been analyzed for the nominal case and for the scenario at t = 20000 s after the DVI line break (where the mass flow rates coming from the SGs are lower, see tab. 1.2), by considering both of the scaling analysis approaches followed, i.e. keeping constant the residence time and the velocity. For each case, simulations considering the grids at the SGs in the FLUENT model (fig. 2.17, fig. 2.19, fig. 2.21, fig. 2.23) and excluding them from the computational domain (fig. 2.16, fig. 2.18, fig. 2.20, fig. 2.22) have been performed.

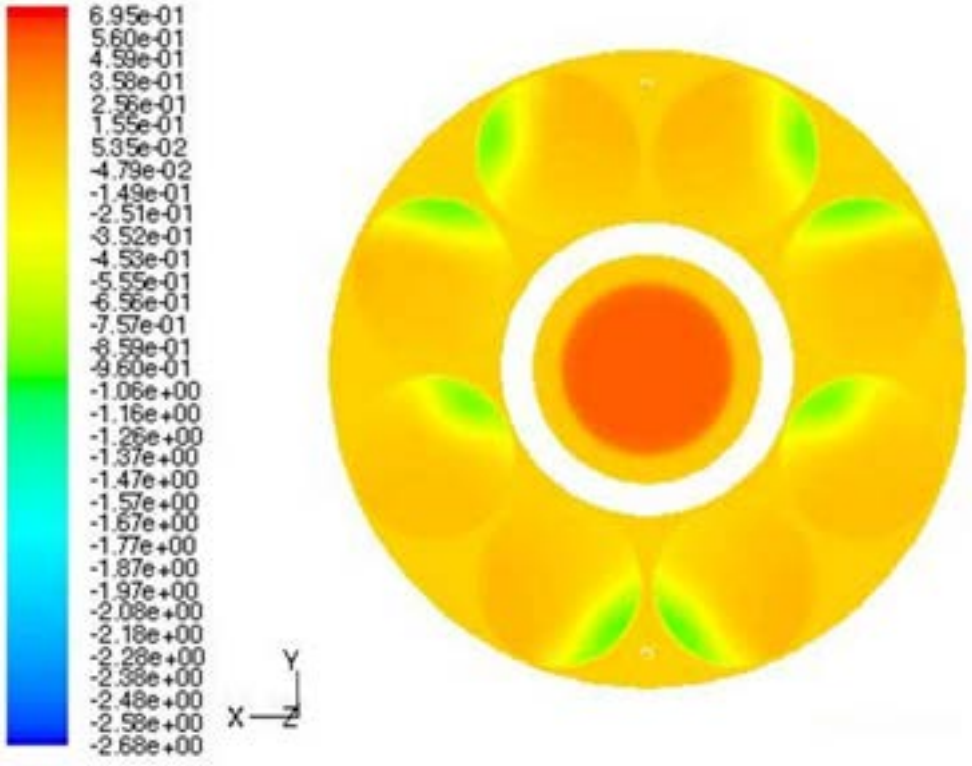

Figure 2.16. *z*-velocity distribution
(nominal case, without grids, constant residence time approach).

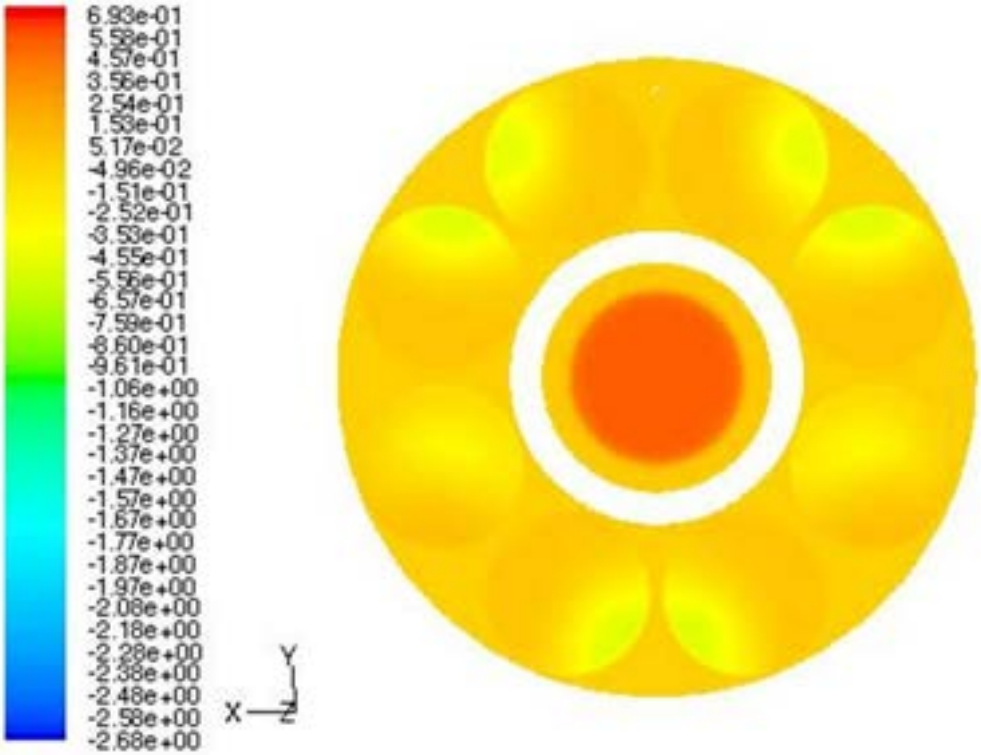

Figure 2.17. *z*-velocity distribution
(nominal case, with grids, constant residence time approach).

For the nominal case (fig. 2.16 and fig. 2.17), it can be observed that the *z*-velocity assumes a more homogeneous profile when grids are considered: even if some differences are still present in the velocity distribution at the section chosen, the velocity profile is less sharp and smoother when the grids are introduced in the computational model (i.e. the green peak values disappear).

The results obtained for the accident case at t = 20000 s (fig. 2.18 and fig. 2.19) show that the effect of the grids does not seem to be so important as for the nominal case, even if a lightly improvement is achieved in order to obtain a smoother velocity distribution. This can be explained by considering the low values of the velocity (up to two order of magnitude lower than in the nominal case), which derive from the lower mass flow rates incoming; so the effect of the grids introduction is less relevant.

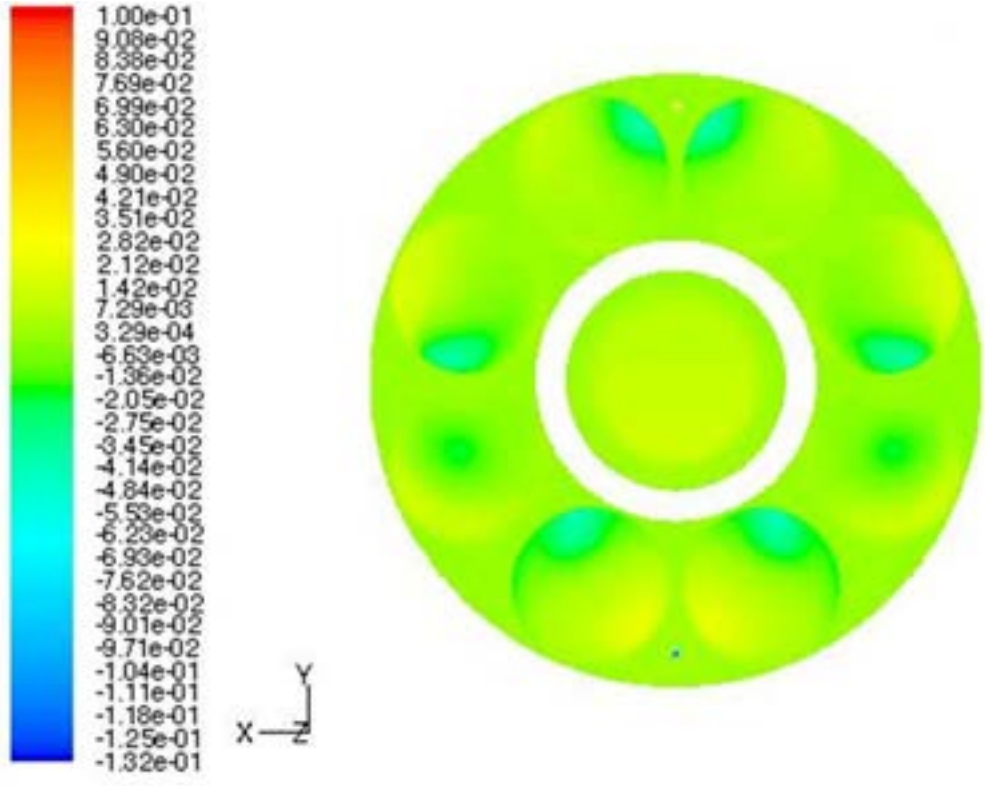

Figure 2.18. *z*-velocity distribution
(t = 20000 s, without grids, constant residence time approach).

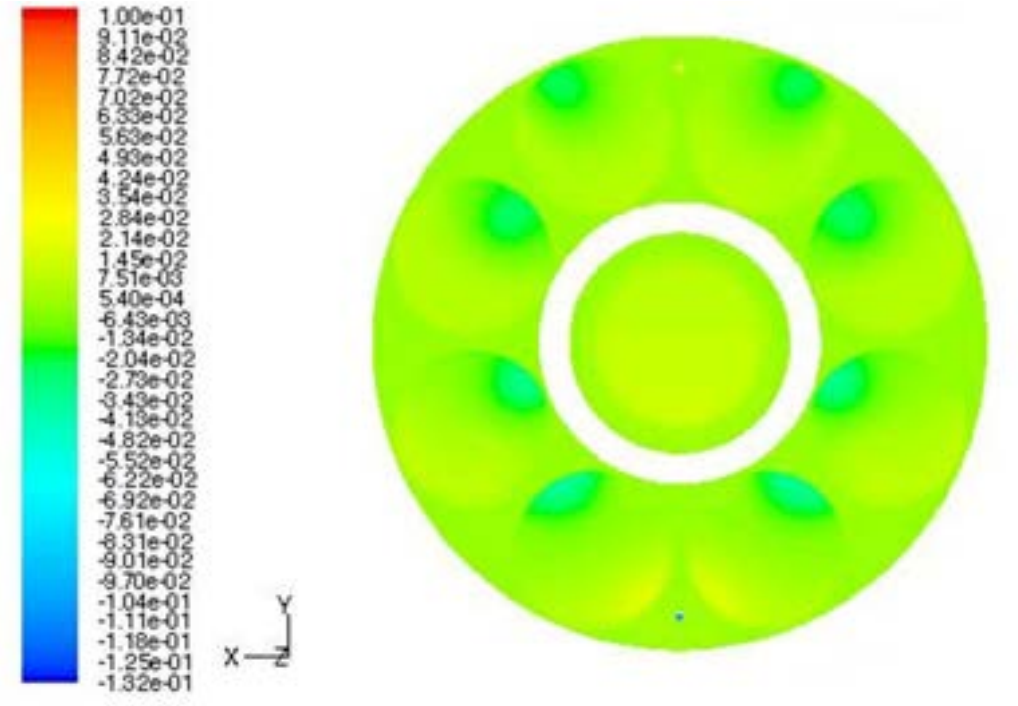

Figure 2.19. *z*-velocity distribution
(*t* = 20000 s, with grids, constant residence time approach).

Analysing the results obtained for the accident case (*t* = 20000 s) by adopting the constant velocity scaling approach (fig. 2.20 and fig. 2.21), we can note that the presence of the grids produces a more homogeneous distribution of the velocity in comparison to what observed using the residence time approach, even if it is still observed a less improvement in comparison to the nominal case (fig. 2.22 and fig. 2.23).

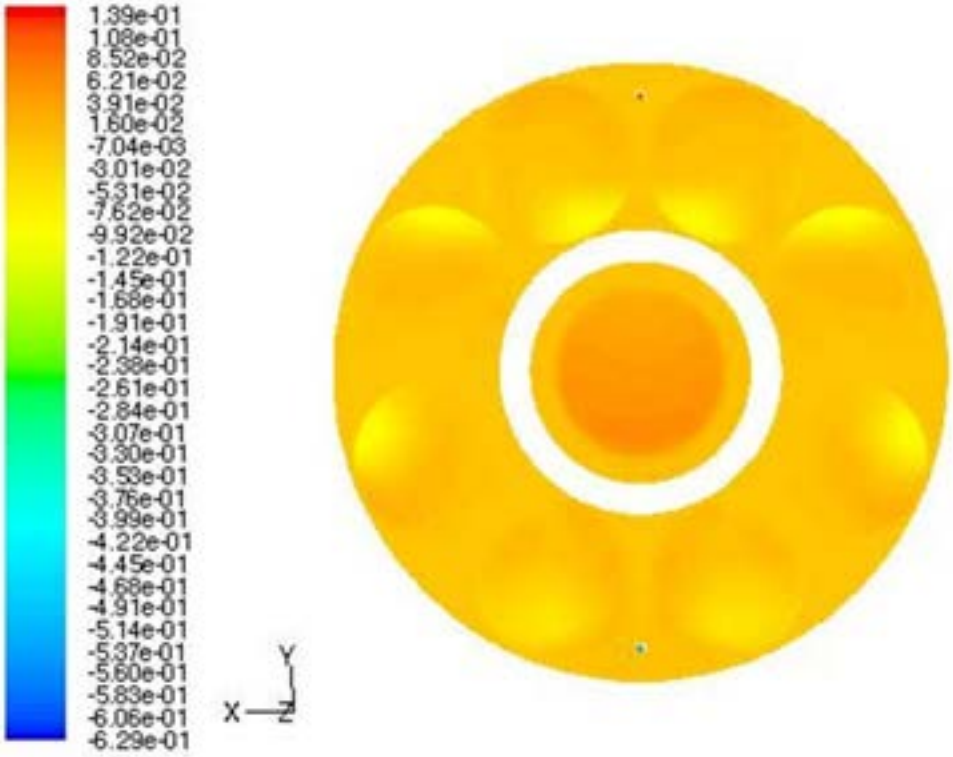

Figure 2.20. *z*-velocity distribution
(*t* = 20000 s, without grids, constant velocity approach).

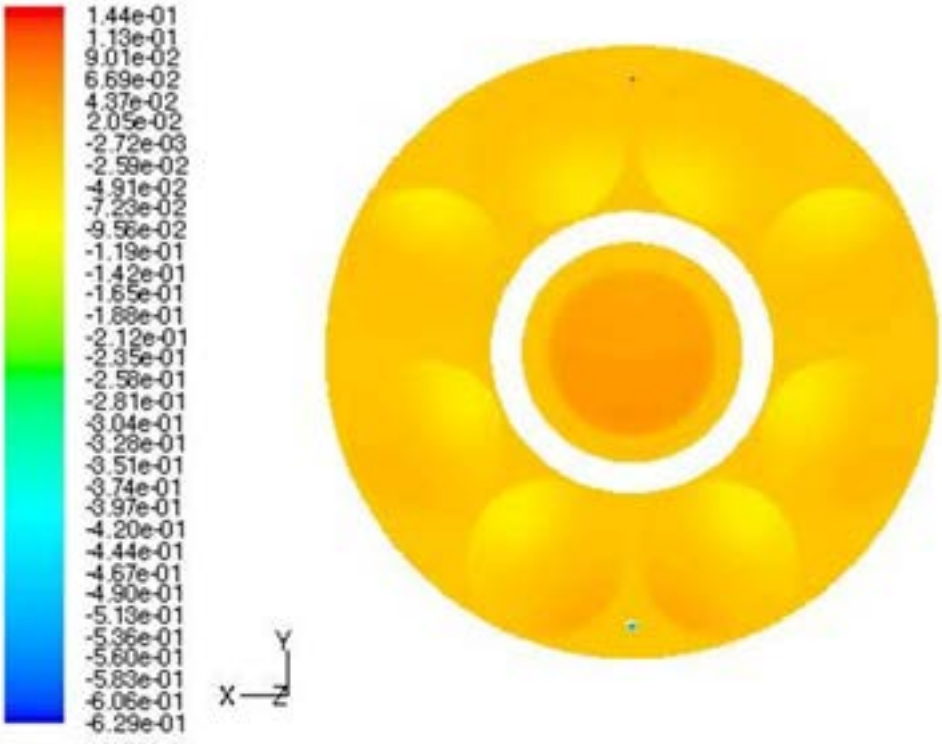

Figure 2.21. *z*-velocity distribution
(*t* = 20000 s, with grids, constant velocity approach).

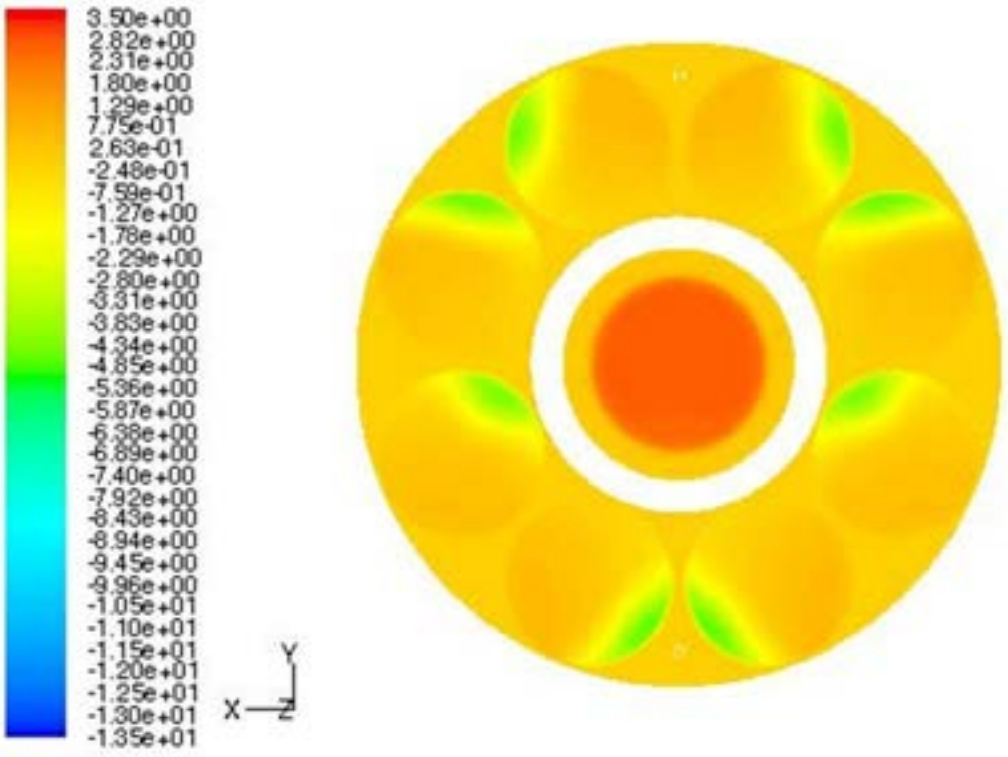

Figure 2.22. *z*-velocity distribution
(nominal case, without grids, constant velocity approach).

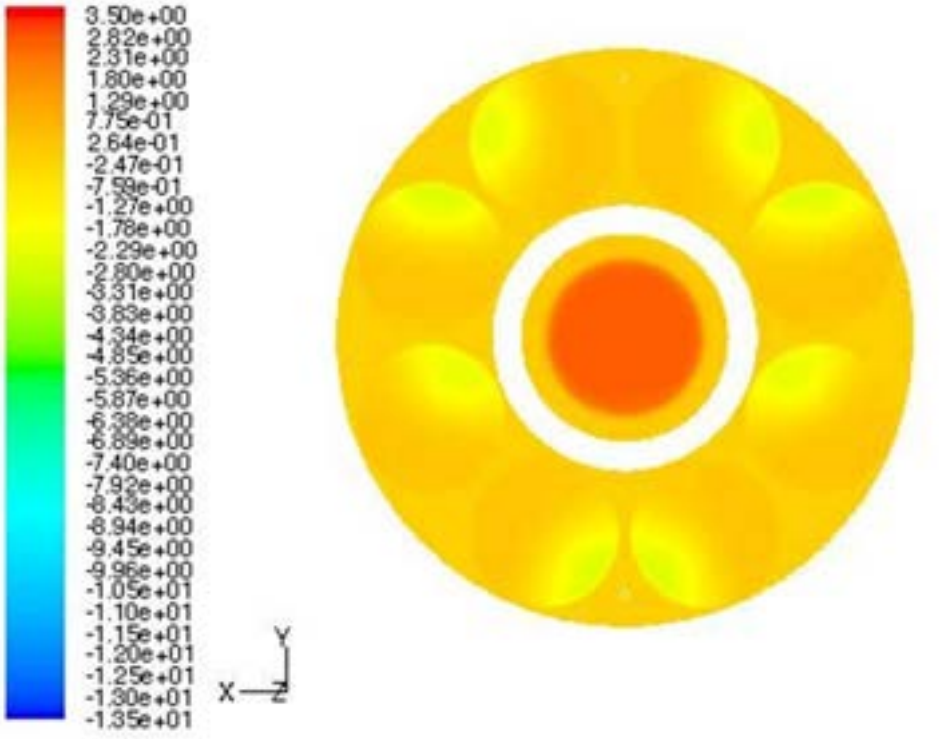

Figure 2.23. *z*-velocity distribution
(nominal case, with grids, constant velocity approach).

3. OBTAINED RESULTS

3.1 Mixing flows analysis in the IRIS downcomer and in the facility

Since the equations which regulate the temperature field and the boron concentration are similar, a qualitative analysis of the mixing processes between the water fluxes from the SGs and the DVI lines, characterized by different temperature, has been performed, following the general approach explained in section 1.2.

Computational simulations have been performed for both the IRIS and the facility model, in order to provide qualitative results concerning the boron concentration in both of the computational domain [7]. The behaviour of both the IRIS model (with and without core supports at the perforated plate) and of the experimental facility have been analyzed for three different time scenarios after a DVI line break accident. It has been analysed the temperature field in the whole reactor and in the facility, in order to figure out the general temperature distribution. Since the boron importance is limited to the reactor core and it is important to know its concentration particularly at the core inlet, the temperature field has been observed at a transverse section of IRIS and of the facility, related to the core inlet. Furthermore, the average values of temperature have been evaluated at the core inlet section and listed in a table. It has to be specified that the average temperature has been obtained by FLUENT post processing panel, by considering the area weighted average integral of the static temperature, evaluated considering only the free surface of the perforated plate below the core at the core inlet for IRIS and the whole free surface for the facility.

The simulations have been performed excluding the gravity field.

By observing the global temperature fields of IRIS at t = 600 s after the DVI line break (from fig. 3.1 to fig. 3.4), the effect of the presence of the lower core supports is immediately detectable. When supports are not considered in the computational domain, the flow rate coming from the intact DVI line crosses the lower part of the downcomer and it starts to rise only when it encounters the opposite wall of the reactor as shown in fig. 3.1, because of the lower values of pressure at the DVI broken line.

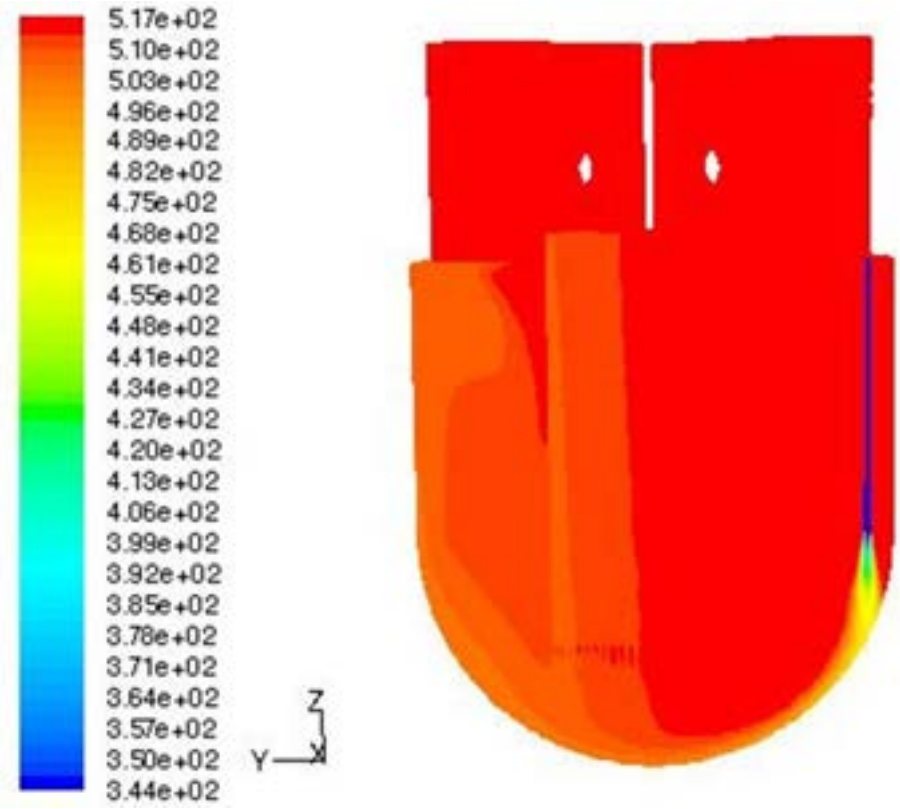

Figure 3.1. Temperature distribution for the IRIS domain
(t = 600 s, without supports).

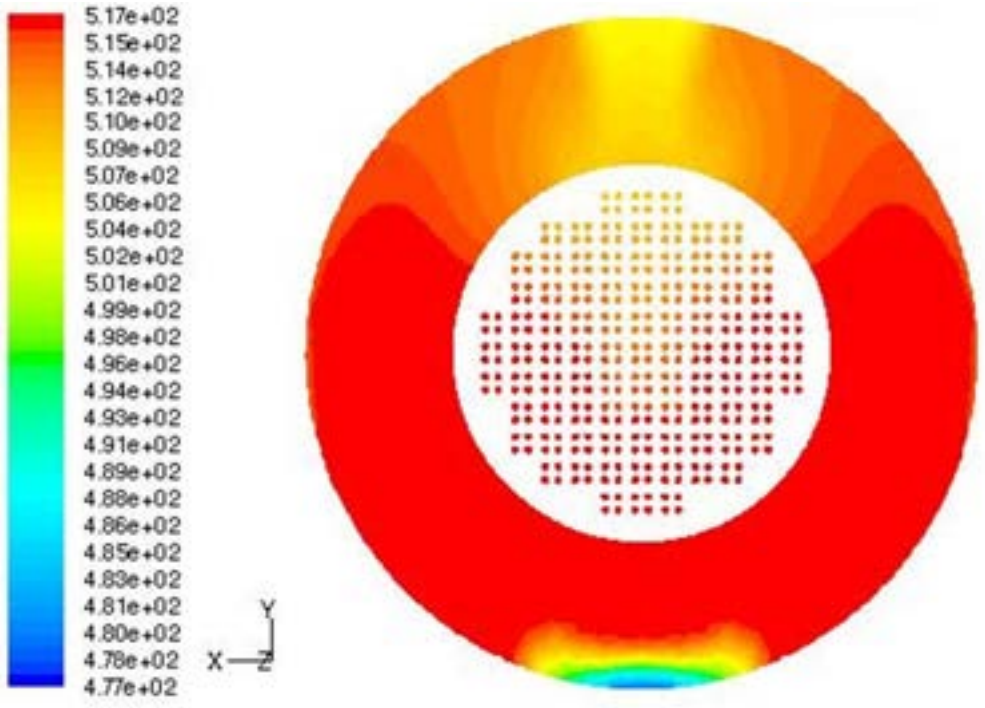

Figure 3.2. Temperature distribution at the core inlet section for the IRIS domain
(t = 600 s, without supports).

On the contrary, the presence of the supports affects the mixing in the lower part of the IRIS downcomer: the flow rate coming from the intact DVI line impacts them, and this reduces the mass flow velocity and improves a more homogeneous temperature distribution into the core.

The comparison between the two configurations can be made from fig. 3.2 and fig. 3.4, which show the transverse temperature distribution in IRIS at the core inlet section.

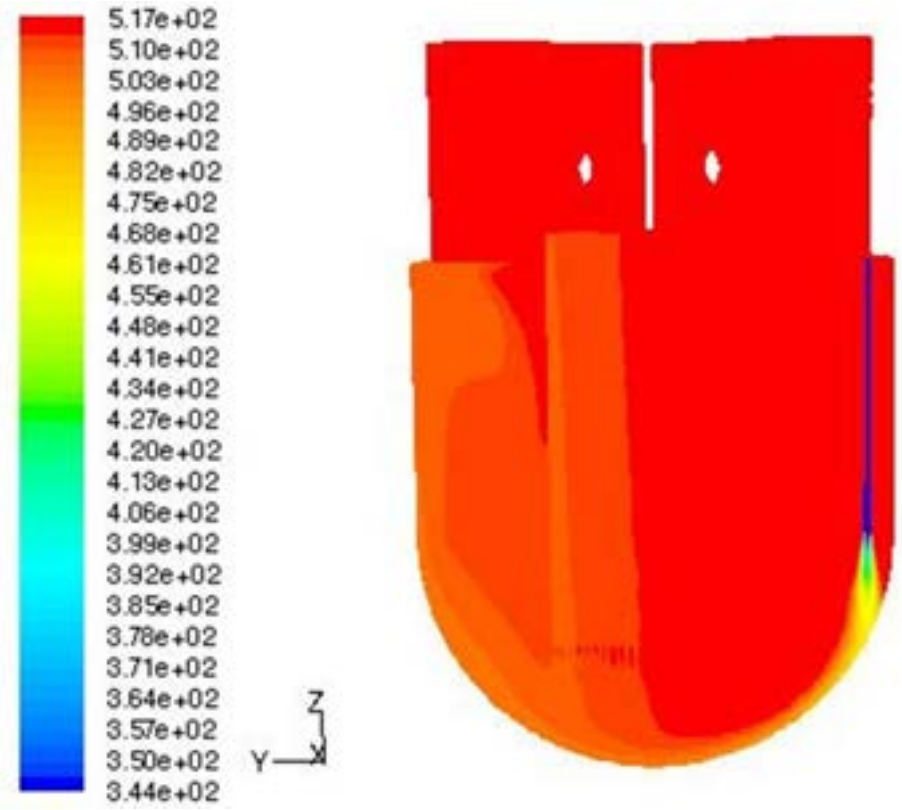

Figure 3.3. Temperature distribution for the IRIS domain
(t = 600 s, with supports).

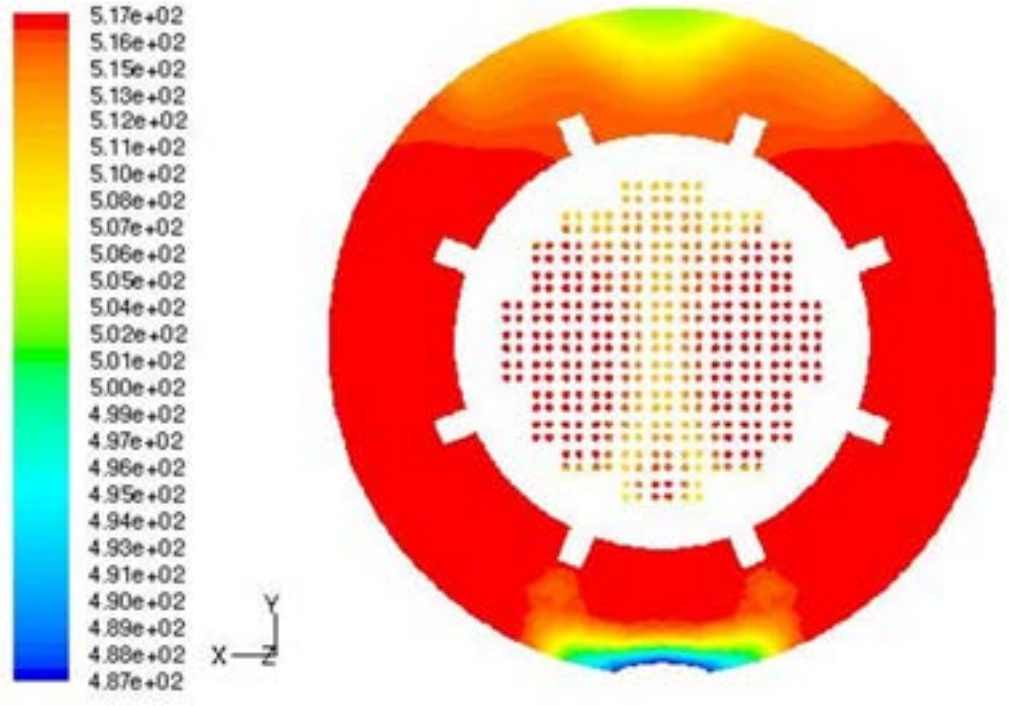

Figure 3.4. Temperature distribution at the core inlet section for the IRIS domain (t = 600 s, with supports).

The average temperature evaluated for the first (supports modelled) IRIS configuration is T = 515.21 K while for the second one (supports not modelled) is T = 515.14 K. Even if the average temperature values are very close to each other, the temperature distribution in the downcomer is definitely different in the two cases, as it can be again noted by a comparison between fig. 3.2 and fig. 3.4.

The temperature distribution for the facility, obtained adopting the constant residence time scaling approach, is shown in fig. 3.5 and in fig. 3.6. Obviously, since no supports and no perforated plate have been considered, the mass flow rate coming from the intact DVI keeps a more regular velocity profile. We can also note that the temperature trend in the facility is qualitatively close to that observed for IRIS when supports are not simulated.

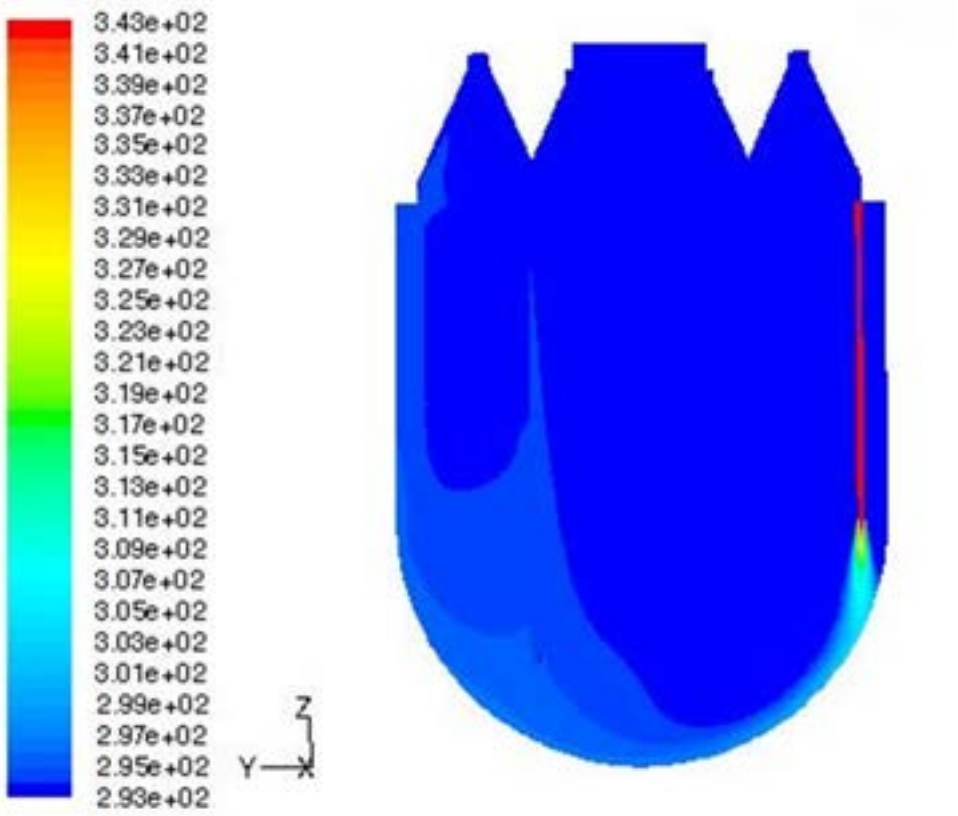

Figure 3.5. Temperature distribution for the facility domain
(t = 600 s, constant residence time approach).

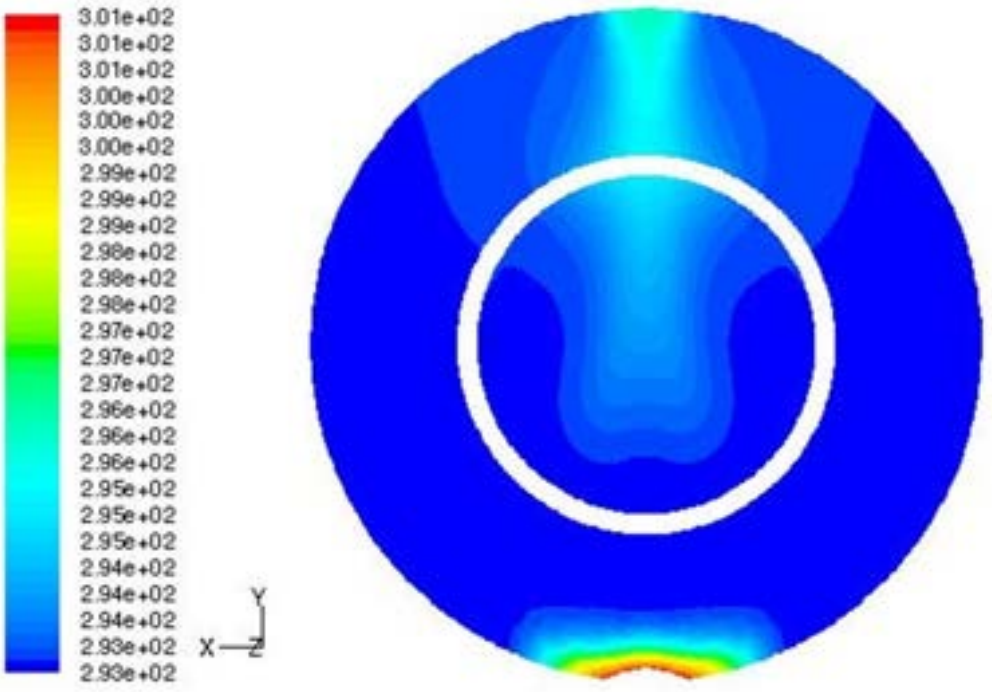

Figure 3.6. Temperature distribution at the core inlet section for the facility domain
(t = 600 s, constant residence time approach).

Following the constant velocity scaling approach (fig. 3.7 and fig. 3.8), a temperature distribution very similar to that observed with the constant residence time approach is achieved. This is also confirmed by making a comparison between the average temperature obtained for the constant residence time scaling criterion (T = 293.54 K) and the constant velocity (T = 293.55 K) one.

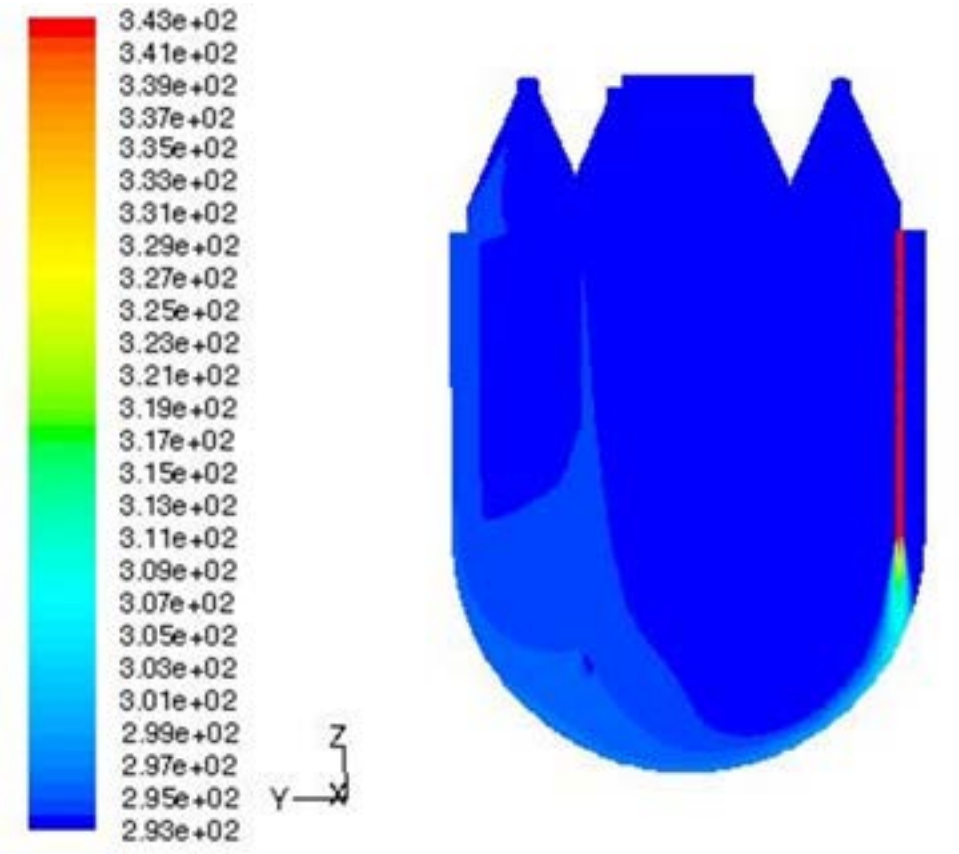

Figure 3.7. Temperature distribution for the facility domain
(t = 600 s, constant velocity approach).

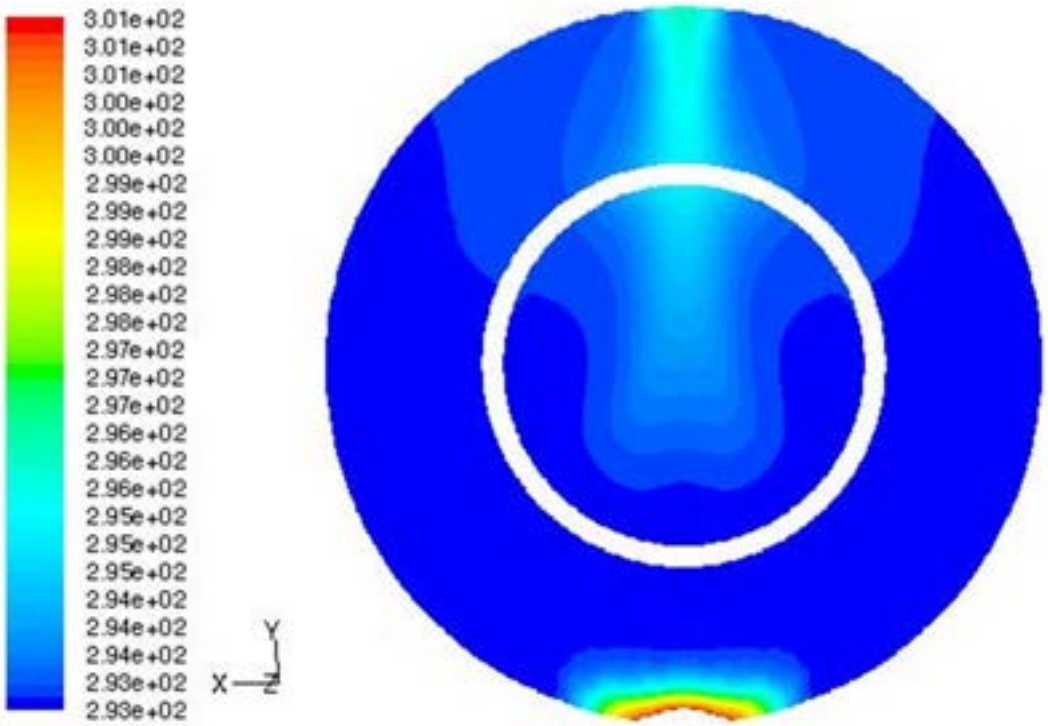

Figure 3.8. Temperature distribution at the core inlet section for the facility domain (t = 600 s, constant velocity approach).

The temperature distributions obtained for IRIS, concerning the temporal scenario at t = 20000 s after the DVI line break, are shown from fig. 3.9 to fig. 3.12. Again, there have been considered both the computational domains with and without the core supports. As previously noted, the presence of the core supports deviates part of the flow rate from the intact DVI and a larger volume of the downcomer is interested by the DVI water than that observed for the configuration without supports; this can be seen by a comparison between fig. 3.9 and fig. 3.11. Moreover the analysis of the profiles at the core inlet section shows a more homogeneous temperature distribution in comparison to that noted above for the temporal scenario at t = 600 s after the DVI line break, both for the configurations with and without core supports (fig. 3.10 and fig. 3.12).

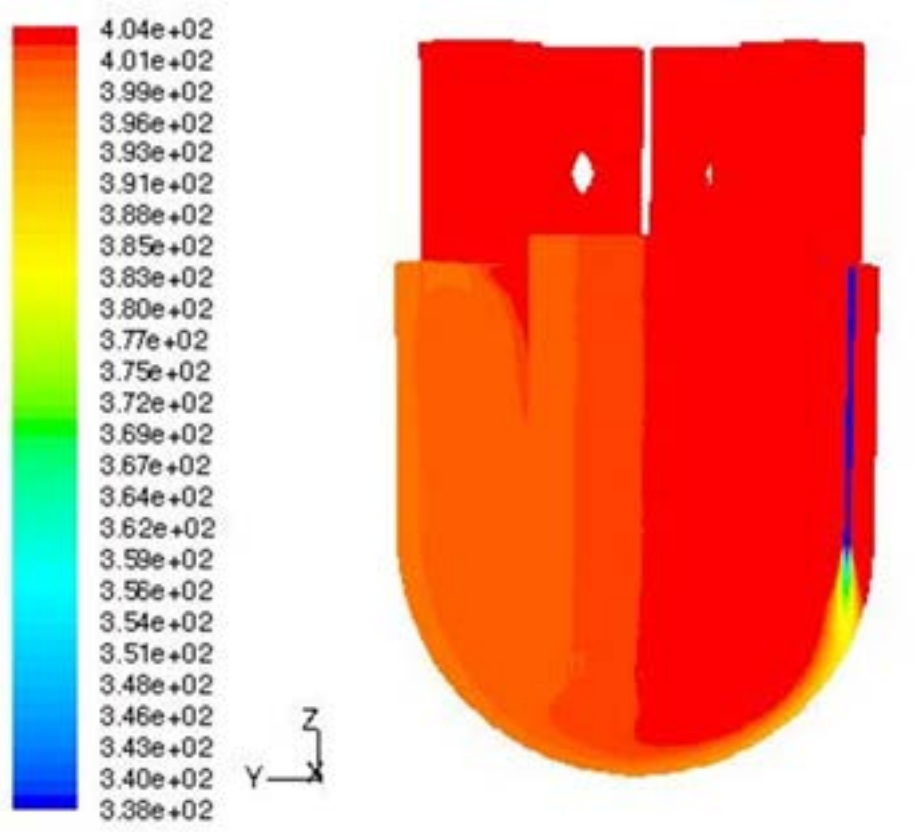

Figure 3.9. Temperature distribution for the IRIS domain
(t = 20000 s, without supports).

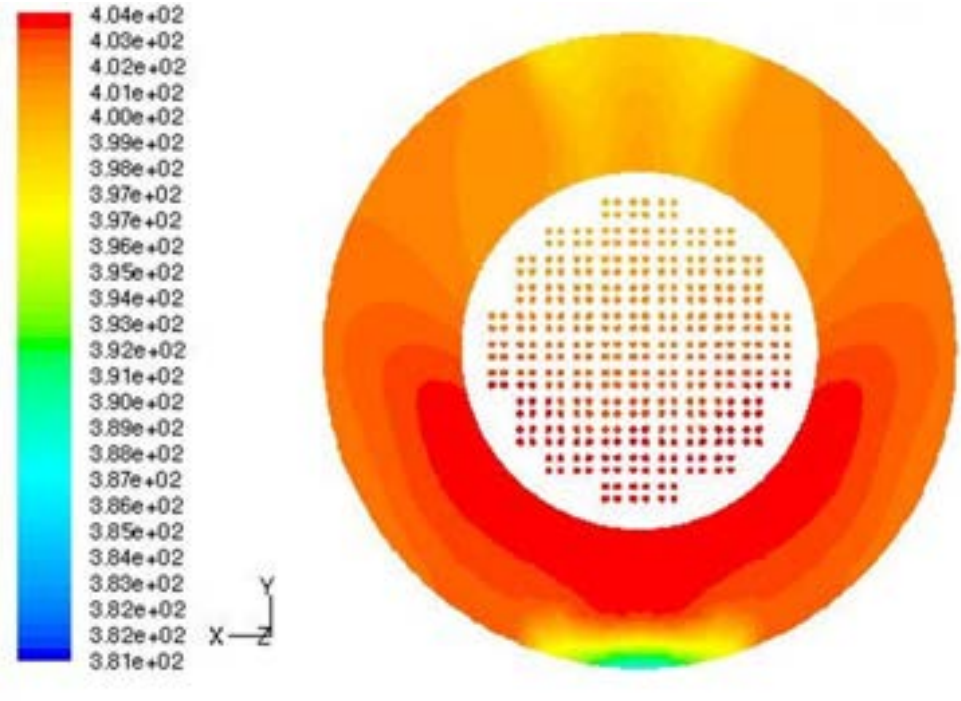

Figure 3.10. Temperature distribution at the core inlet section for the IRIS domain
(t = 20000 s, without supports).

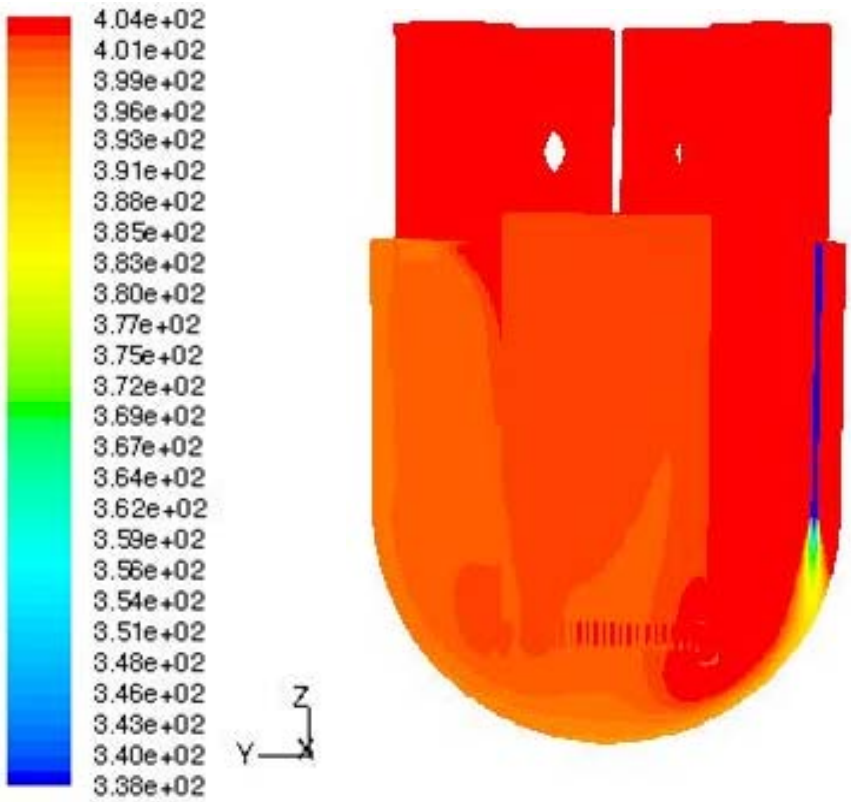

Figure 3.11. Temperature distribution for the IRIS domain
(t = 20000 s, with supports).

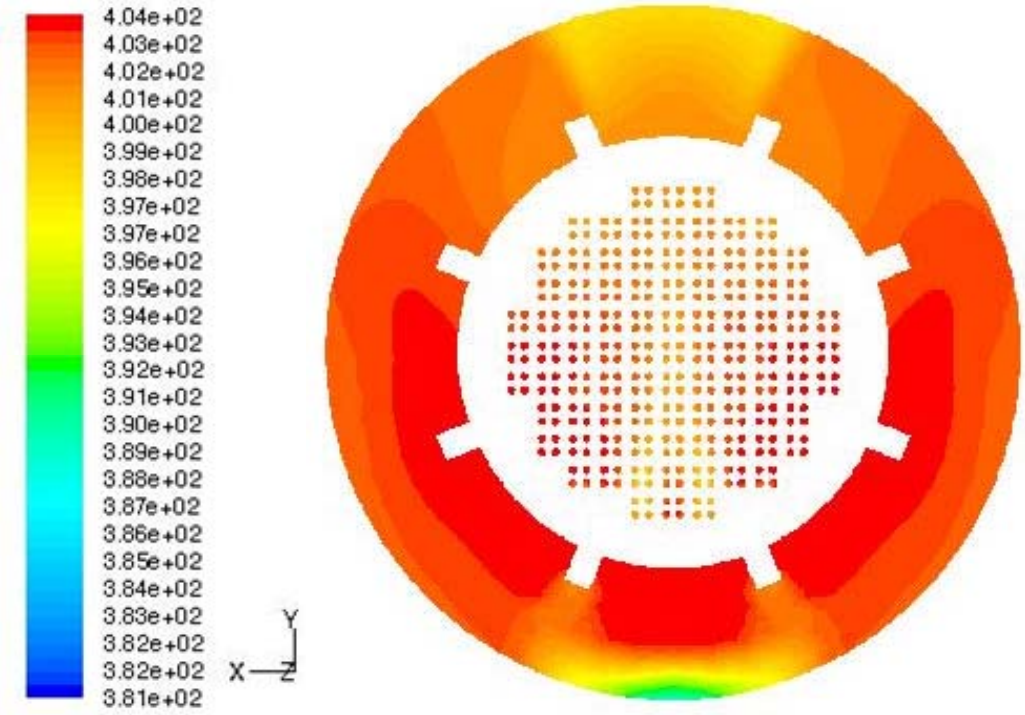

Figure 3.12. Temperature distribution at the core inlet section for the IRIS domain
(t = 20000 s, with supports).

The average value of temperature at the core inlet section is T = 402.63 K for the configuration without core supports, while a value of T = 402.65 K is calculated for the simulation with core supports.

Concerning the facility results obtained for the simulation run at t = 20000 s after the DVI line break (from fig. 3.13 to fig. 3.16), it can be noted that different temperature profiles are achieved, depending to the scaling approach adopted and in comparison to the results obtained for the simulation performed for t = 600 s. In fact, since the mass flow rate from the DVI for t = 20000 s is smaller than that for t = 600 s (see tab 1.2), performing simulations with different scaling approaches greatly affects the magnitude of the mass flow rate coming into facility from the SGs. In particular, when the residence time is conserved, smaller mass flow rates are considered and this causes relevant mixing processes only in a limited zone of the internal cylinder simulating the core, in the lower part of the facility.

We can see that with the constant residence time approach, we have only a small part of the facility interested by the DVI mass flow rate (fig. 3.13), while the adoption of the constant velocity approach allows to have a larger part of the facility interested by the DVI water, as shown in fig. 3.15. The comparison between the temperature distribution in the transversal section at the core inlet confirms that the adoption of the constant velocity scaling method allows a more homogeneous temperature distribution.

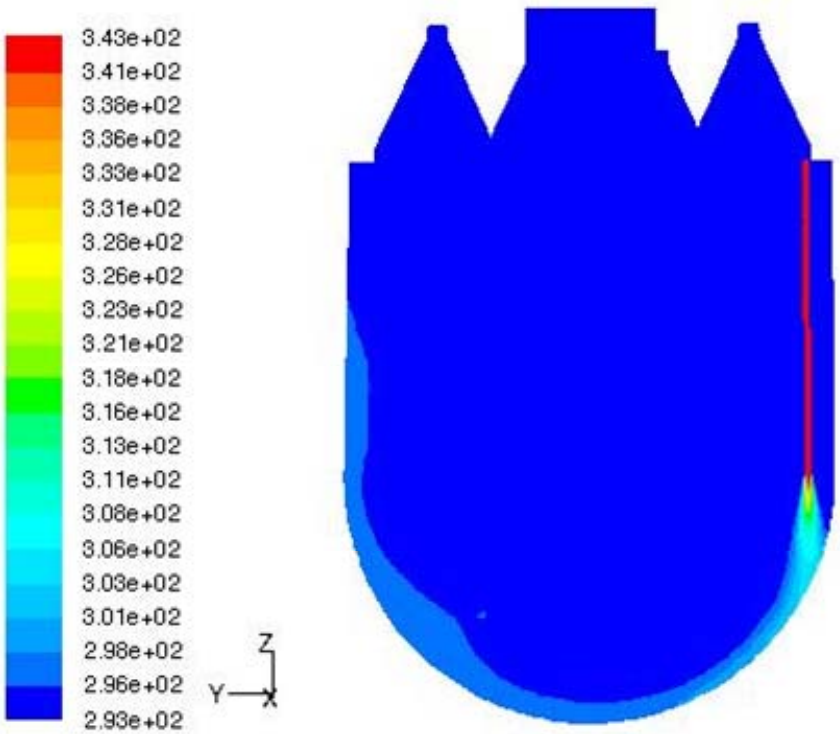

Figure 3.13. Temperature distribution for the facility domain
(*t* = 20000 s, constant residence time approach).

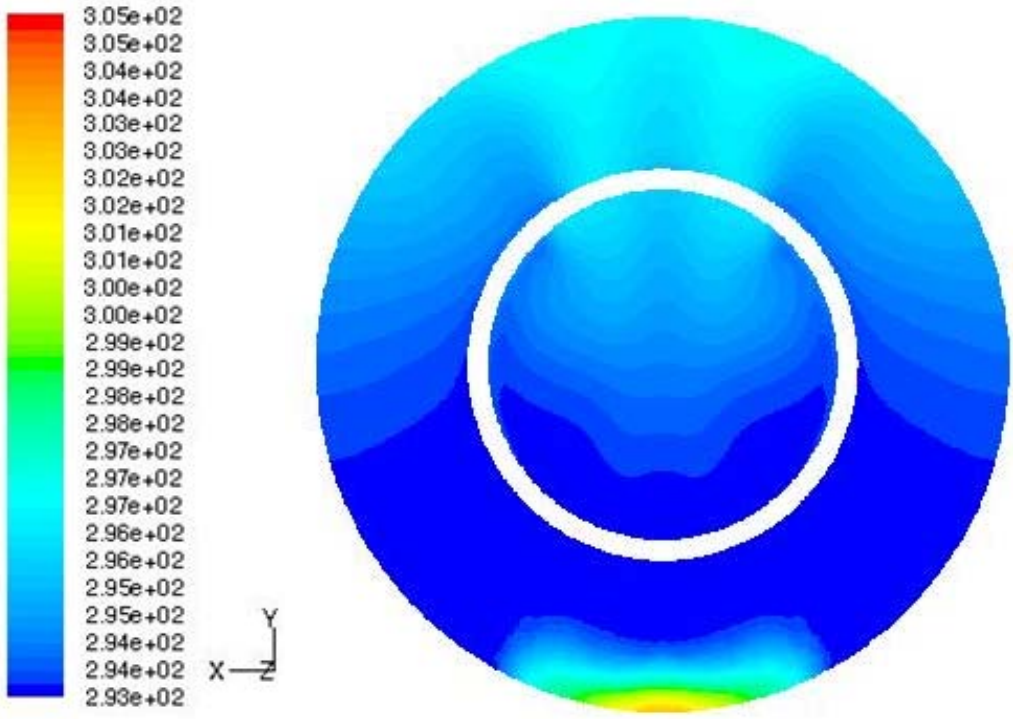

Figure 3.14. Temperature distribution at the core inlet section for the facility domain
(*t* = 20000 s, constant residence time approach).

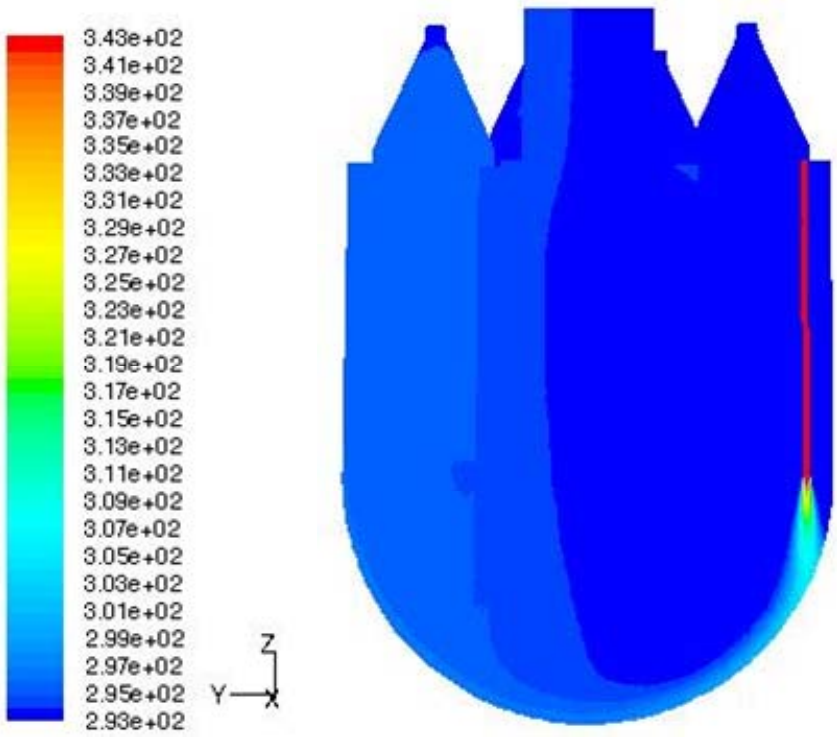

Figure 3.15. Temperature distribution for the facility domain
(t = 20000 s, constant velocity approach).

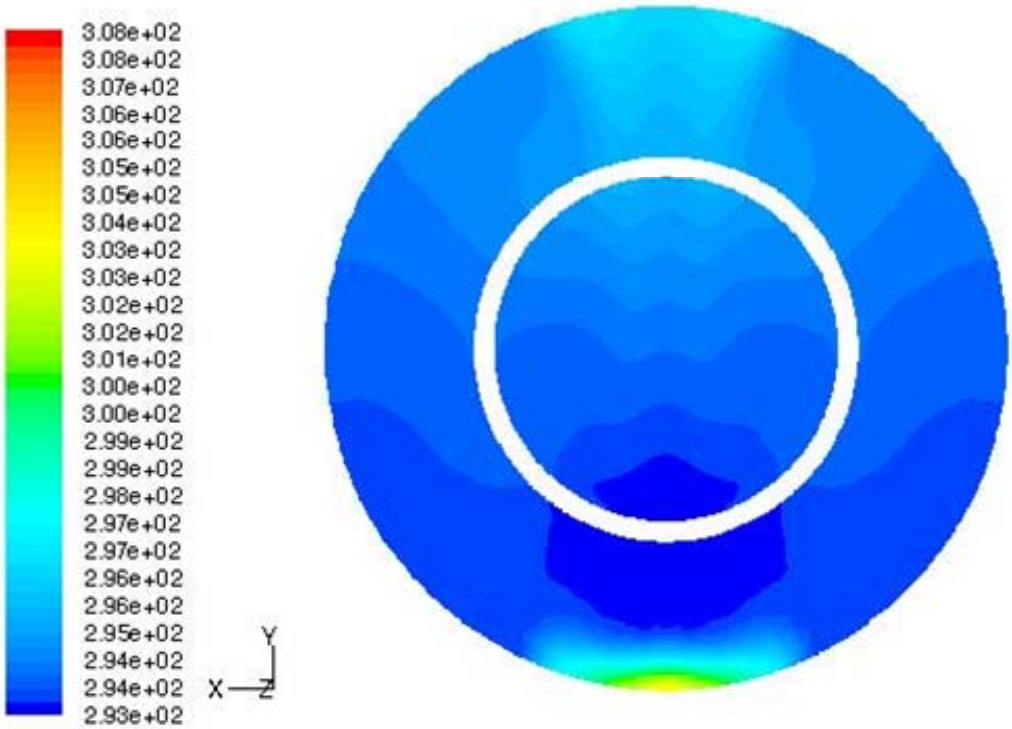

Figure 3.16. Temperature distribution at the core inlet section for the facility domain
(t = 20000 s, constant velocity approach).

The average temperatures for the facility, measured at the core inlet section, are T = 294.06 K and T = 294.10 K for the constant residence time and for the constant velocity scaling approaches, respectively.

The last case proposed is referred to the time window at t = 60000 s after the beginning of the transient due to the DVI line accident.

Considering the IRIS model, the DVI line break changes its mass flow direction, i.e. it starts injecting in the downcomer because the reactor internal pressure is strongly decreased (from 15.5 MPa at the nominal conditions to about 0.3 MPa). This effect is shown from fig. 3.17 to fig. 3.20, for both the configurations without and with supports, respectively.

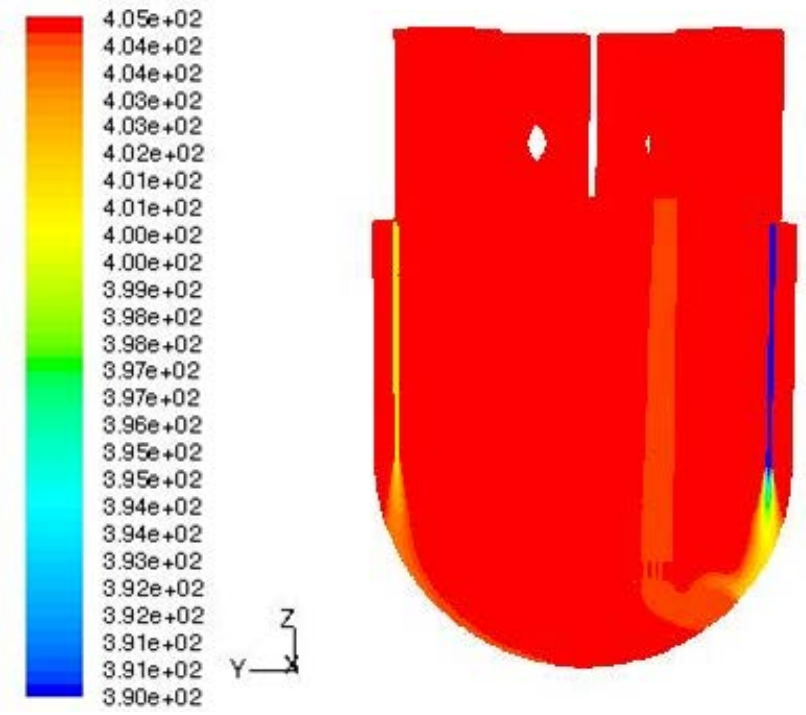

Figure 3.17. Temperature distribution for the IRIS domain (t = 60000 s, without supports).

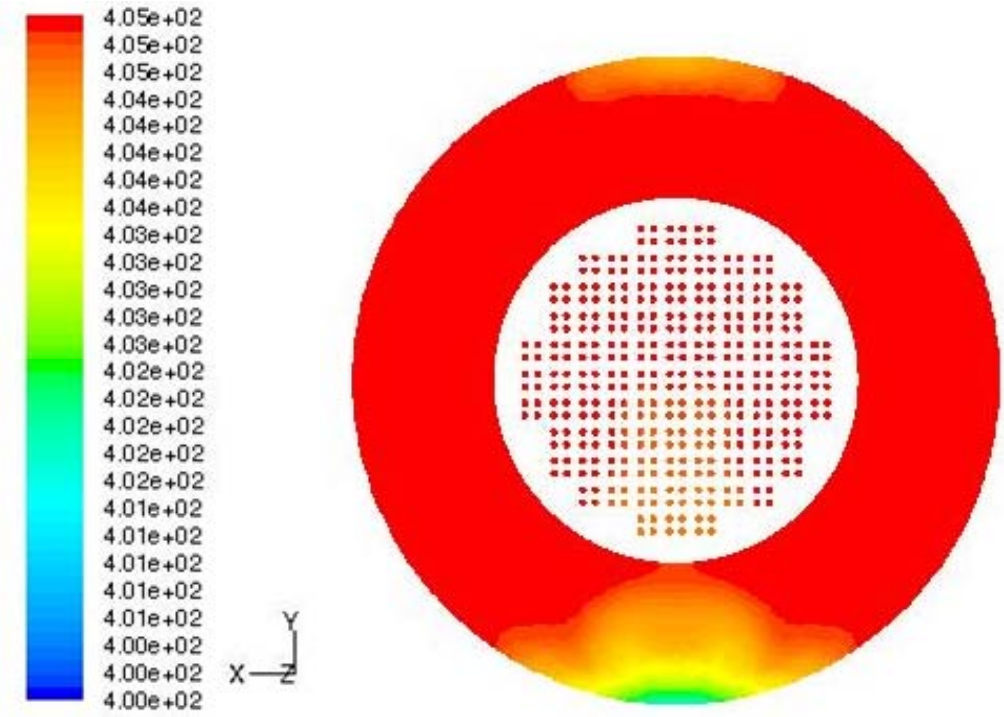

Figure 3.18. Temperature distribution at the core inlet section for the IRIS domain (t = 60000 s, without supports).

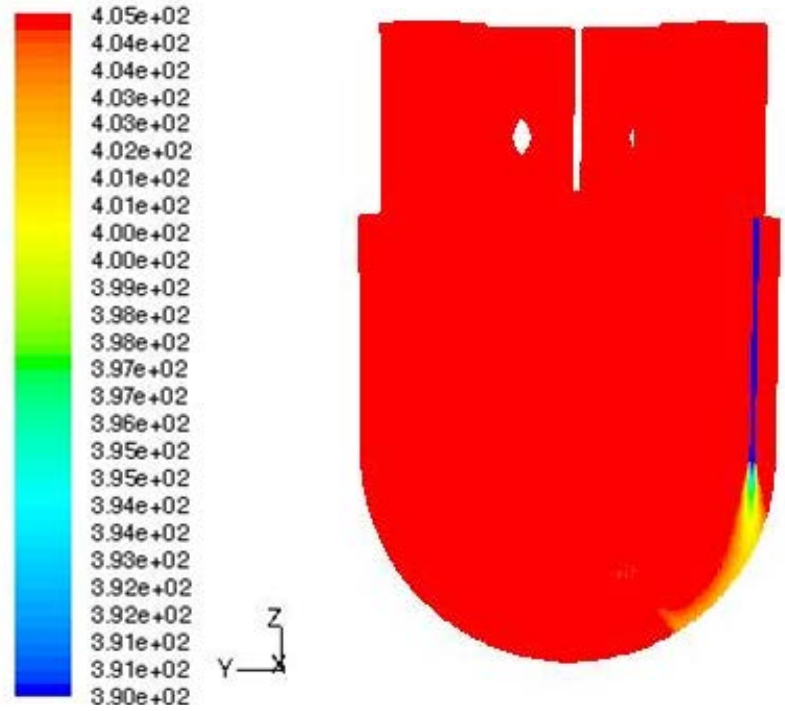

Figure 3.19. Temperature distribution for the IRIS domain (t = 60000 s, with supports).

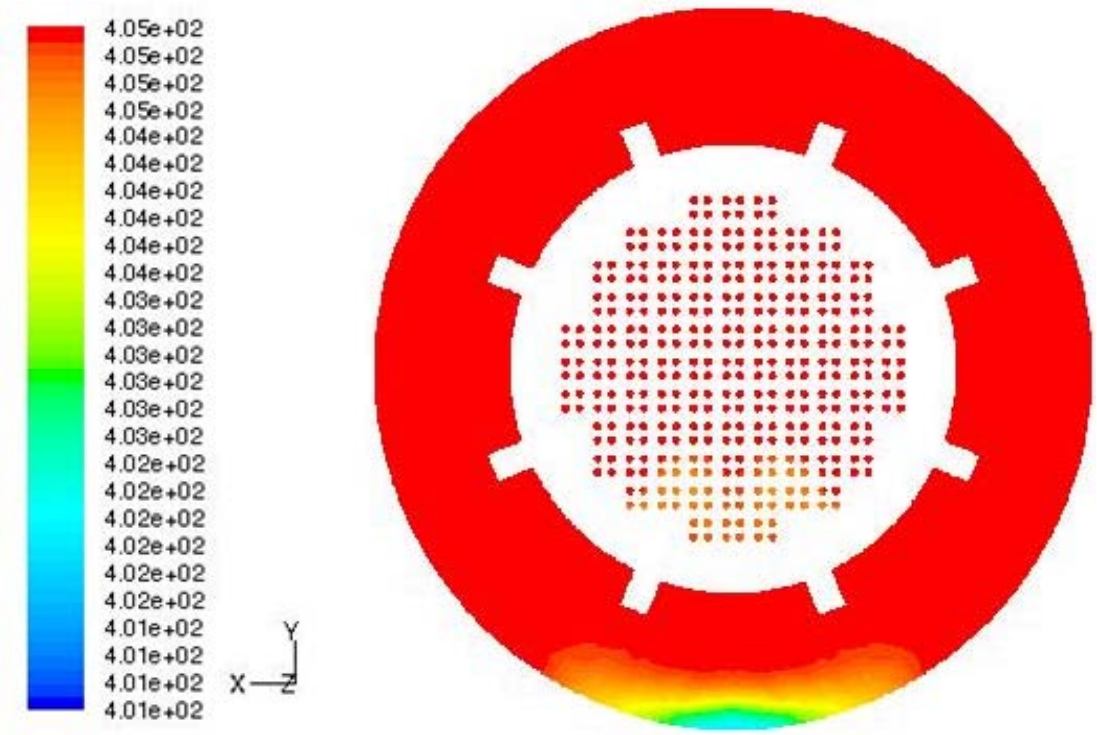

Figure 3.20. Temperature distribution at the core inlet section for the IRIS domain (t = 60000 s, with supports).

As already mentioned both of the DVI lines are injecting, but one of the injections is about 2.5 time higher than the other one and this produces as result the temperature profiles obtained in the IRIS inlet core section observable in fig. 3.18.

For the simulation without core supports, the average temperature in the core inlet section is T = 402.63 K, while including the core supports in the model the average temperature is T = 402.65 K. Again it is noted a more homogeneous temperature distribution for the configuration with the core supports.

Also the facility behaviour has been analysed for the time window at t = 60000 s after the DVI line break, both for the constant residence time scaling approach (fig. 3.21 and fig. 3.22) and for the constant velocity scaling approach (fig. 3.23 and fig. 3.24). We can observe that in these simulations both the DVI line inject flow rates of the same order of magnitude and so the temperature distribution are almost similar for both the scaling approaches adopted.

Concerning the average temperatures, T = 294.05 K for the constant residence time approach and T = 294.10 K for the velocity scaling approach has been calculated.

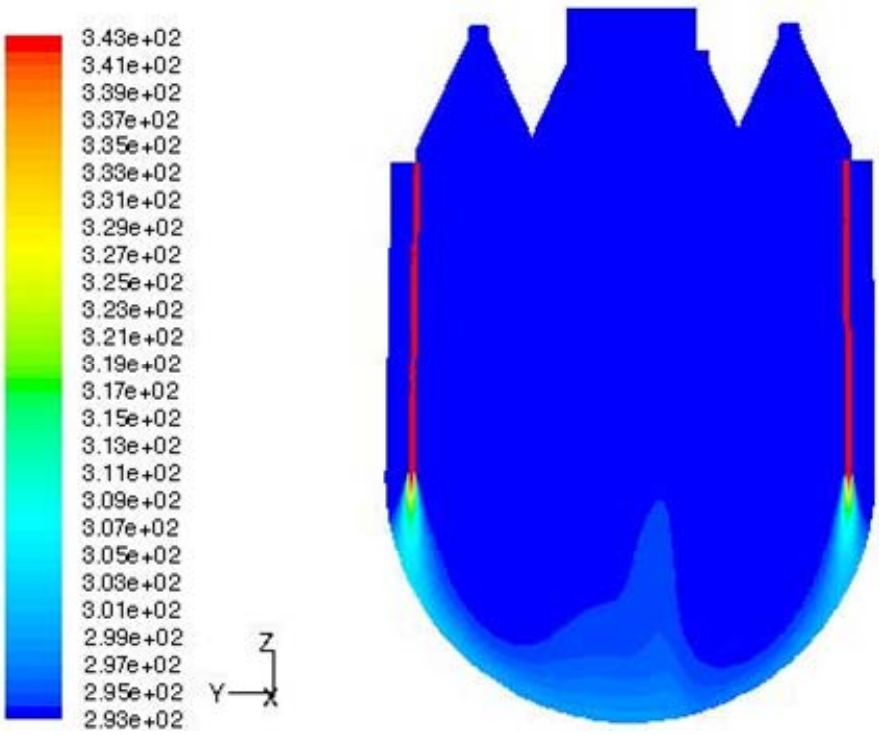

Figure 3.21. Temperature distribution for the facility domain
(t = 60000 s, constant residence time approach).

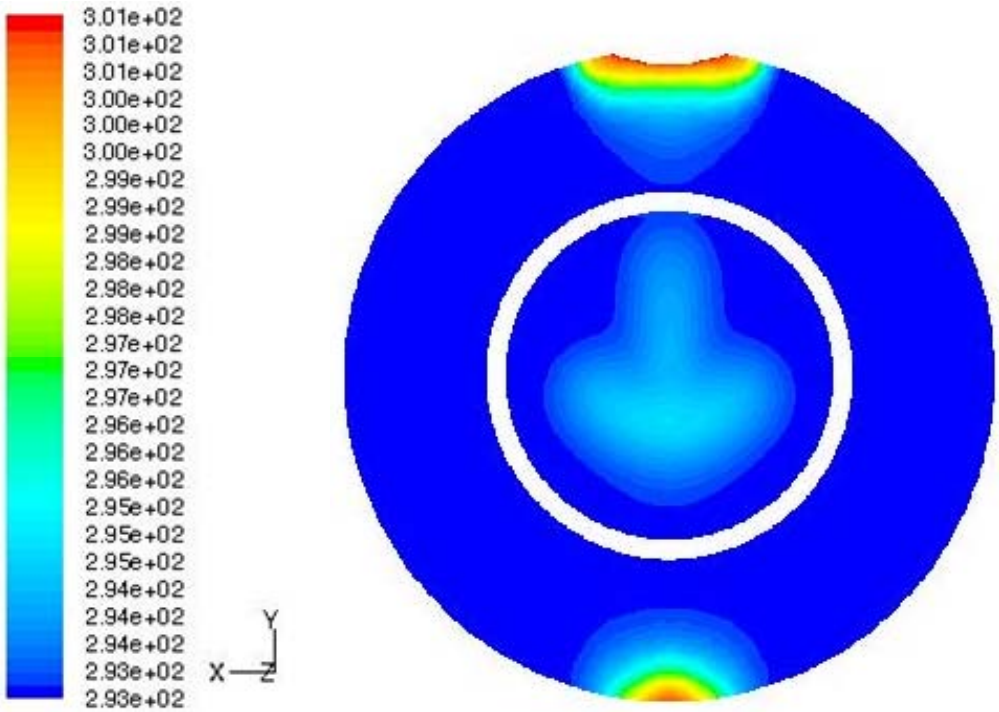

Figure 3.22. Temperature distribution at the core inlet section for the facility domain
(t = 60000 s, constant residence time approach).

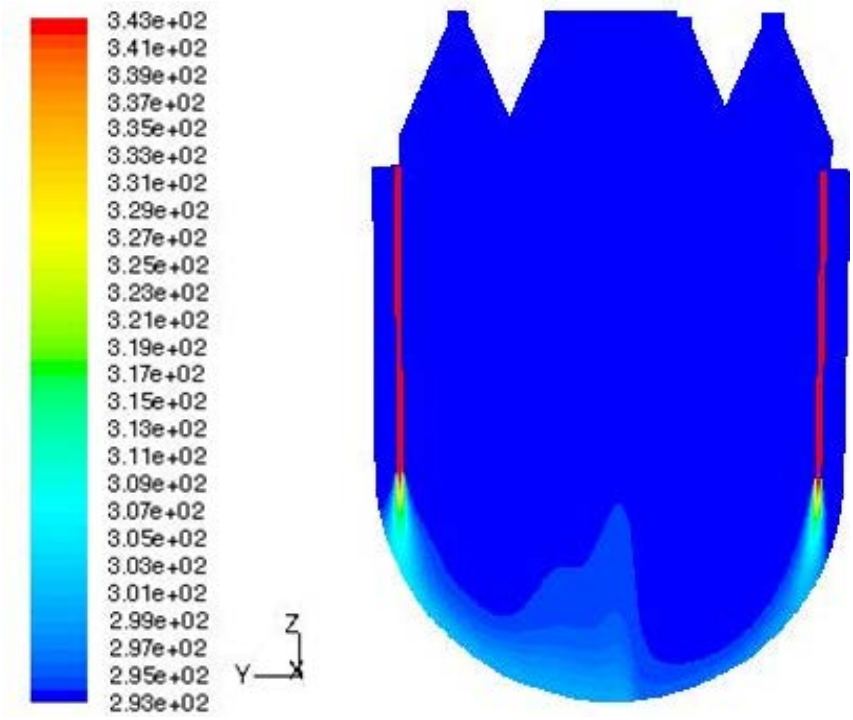

Figure 3.23. Temperature distribution for the facility domain
(t = 60000 s, constant velocity approach).

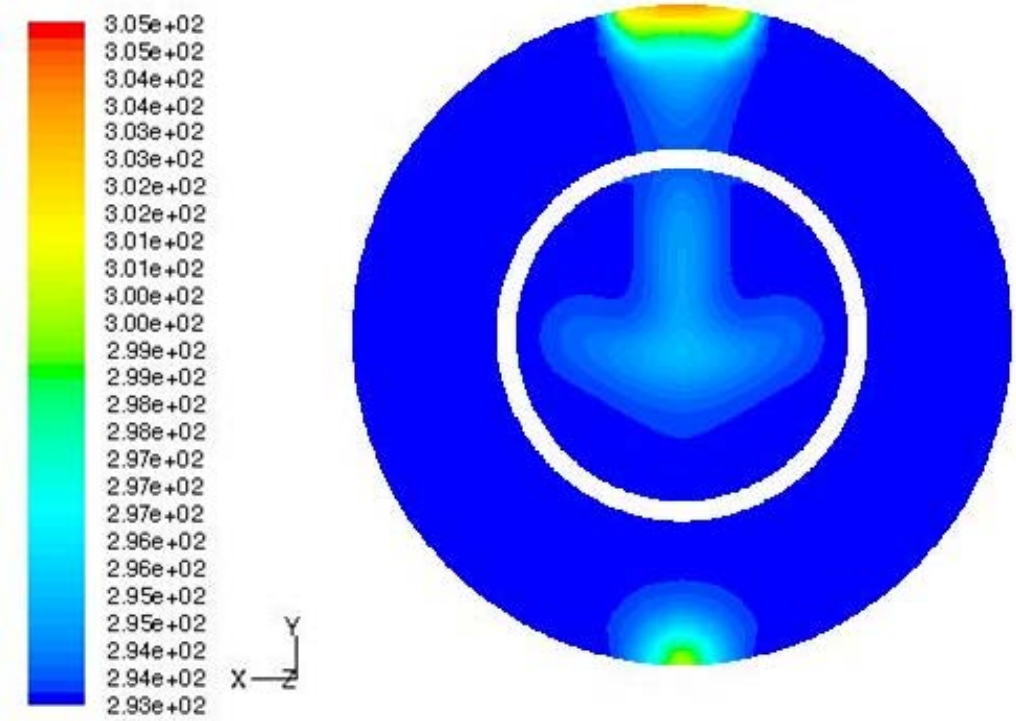

Figure 3.24. Temperature distribution at the core inlet section for the facility domain
(t = 60000 s, constant velocity approach).

In order to get a better comparison between the results from IRIS and from the facility simulations, a non dimensional analysis is proposed. The simple average temperature is not enough to investigate the differences between the different cases simulated, because of the different temperature values adopted during the simulations for IRIS and the facility models which can greatly affect the final results. A non dimensional temperature can be specified as follow [3]:

$$T^* = \frac{T - T_{DC}}{T_{DVIin} - T_{DC}}$$

where:

T is the evaluated average temperature;
T_{DC} is the downcomer temperature (SGs inlet temperature);
T_{DVIin} is the DVI injection water temperature.

The non dimensional values of temperature are collected in tab. 3.1.

Non dimensional *T*				
Time [s]	***IRIS without supports***	***IRIS with supports***	***FACILITY (constant residence time)***	***FACILITY (constant velocity)***
600	9.98E-03	1.04E-02	7.84E-03	7.90E-03
20000	2.15E-02	2.13E-02	1.81E-02	1.90E-02
60000	5.20E-02	4.81E-02	8.44E-03	8.47E-03

Table 3.1. Non dimensional *T* for the IRIS and the facility domains, for different temporal windows after the DVI line break event.

As it can be noted from table 3.1, the non dimensional temperatures in IRIS are in a good agreement with those calculated for the facility during the first two temporal windows considered (t = 600 s and t = 20000 s). In particular, better results have been obtained when the scaling analysis is performed adopting the constant velocity scaling approach. A lower agreement between the simulations, almost an order of magnitude, is observed for the last time window at t = 60000 s.

3.2 The importance of the assumption made for the scaling analysis

In order to perform a scaling analysis between IRIS and the facility some assumptions have been imposed as explained in chapter 1.2. The purpose of this chapter is to consider the importance of these assumptions and to analyse how they can affect the final results; in particular the importance of the absence of gravity will be investigated.

In the following, the role of gravity in the mixing processes is studied, analyzing the velocity component in the *z* coordinate and by comparing the temperature field in the downcomer in the case of gravity presence and when gravity is neglected. This analysis has been developed for all the transient time windows observed, for both IRIS (with and without supports) and the facility (from fig. 3.25 to fig. 3.36).

Furthermore, in IRIS the DVI lines inject water at lower temperature than that coming in the downcomer from the steam generators, while in the facility the DVI lines inject hotter water compared to that injected by the SGs: this discrepancy in the temperature values between IRIS and the facility has been investigated too.

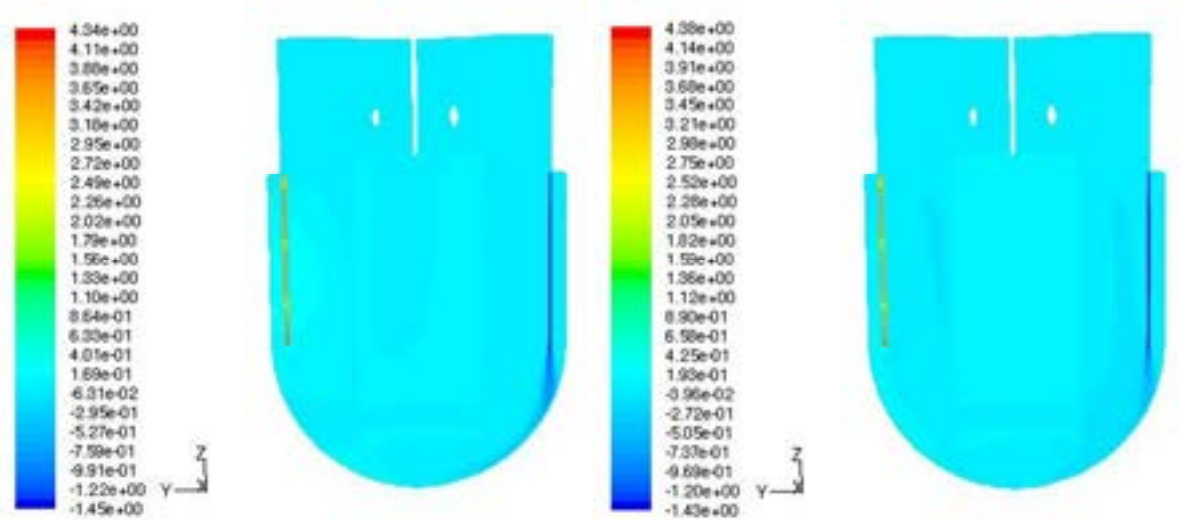

Figure 3.25. *z*-velocity distribution for the IRIS domain
(*t* = 600 s, without supports, with gravity (left) and without gravity (right)).

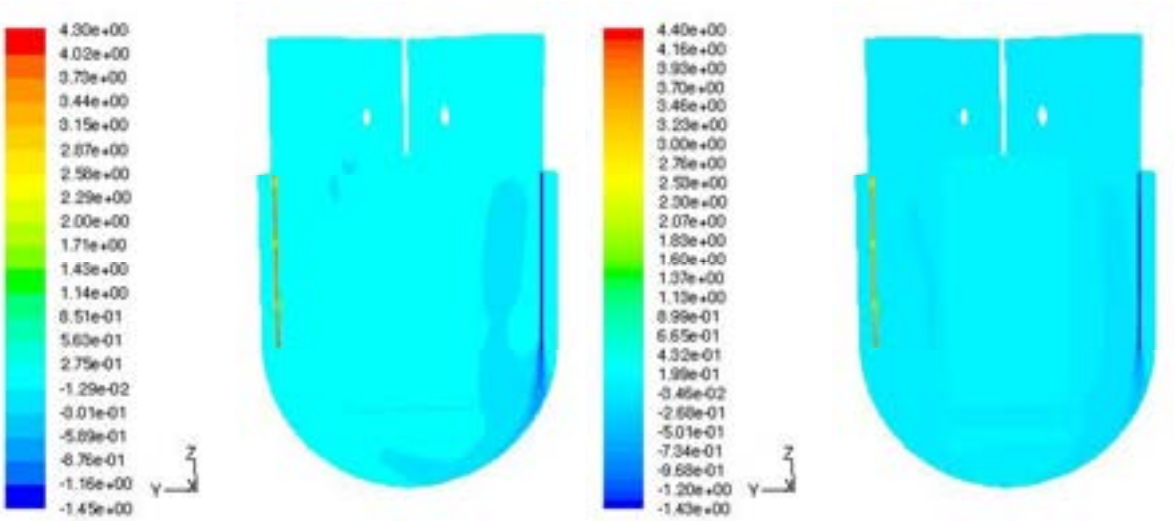

Figure 3.26. *z*-velocity distribution for the IRIS domain
(*t* = 600 s, with supports, with gravity (left) and without gravity (right)).

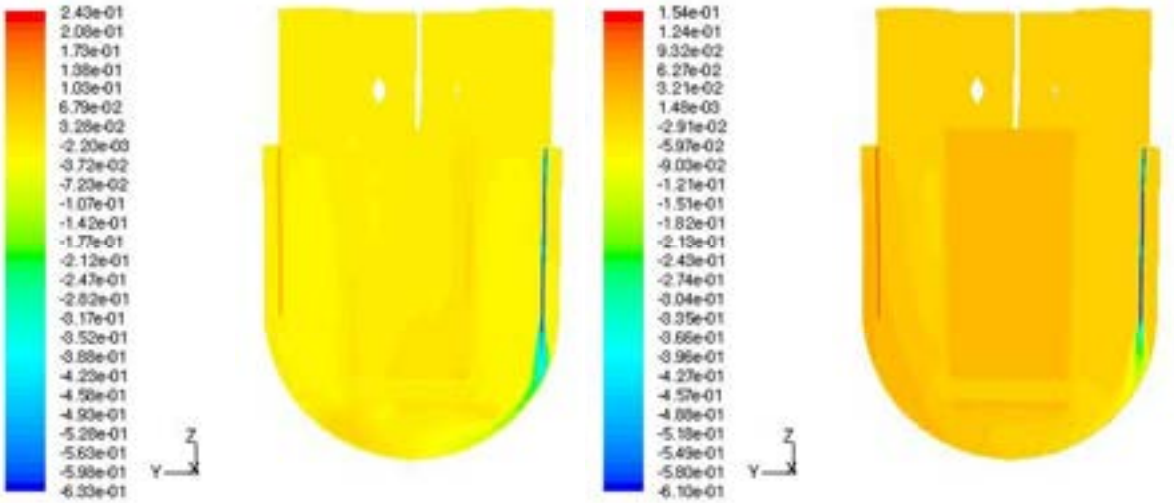

Figure 3.27. *z*-velocity distribution for the IRIS domain
(*t* = 20000 **s**, without supports, with gravity (left) and without gravity (right)).

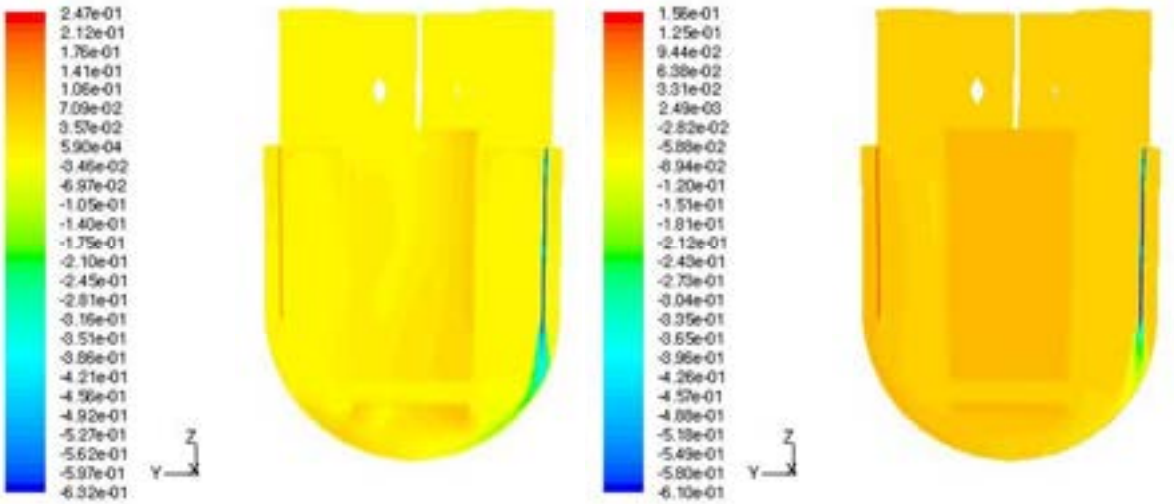

Figure 3.28. *z*-velocity distribution for the IRIS domain
(*t* = 20000 **s,** with supports, with gravity (left) and without gravity (right)).

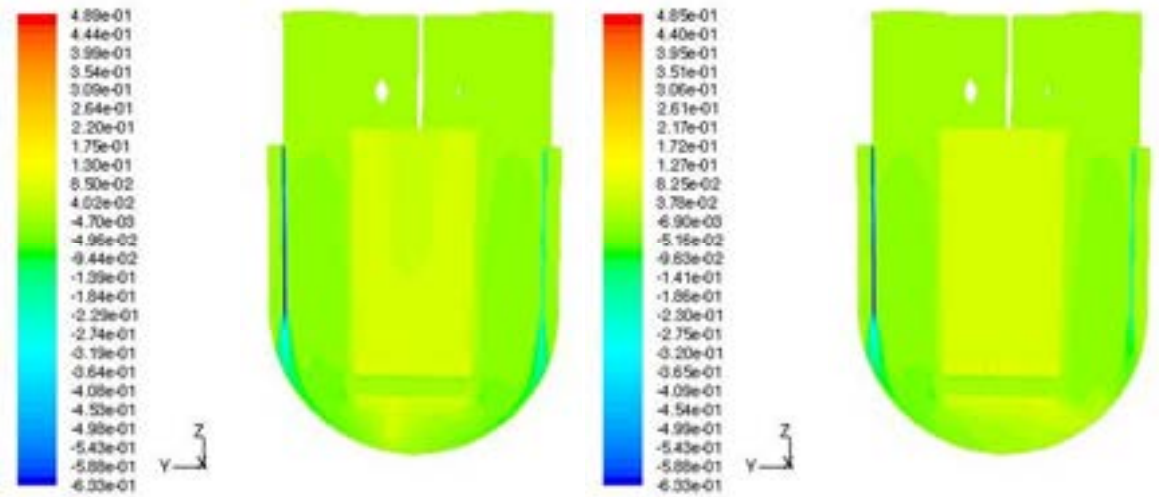

Figure 3.29. *z*-velocity distribution for the IRIS domain
(*t* = 60000 s, without supports, with gravity (left) and without gravity (right)).

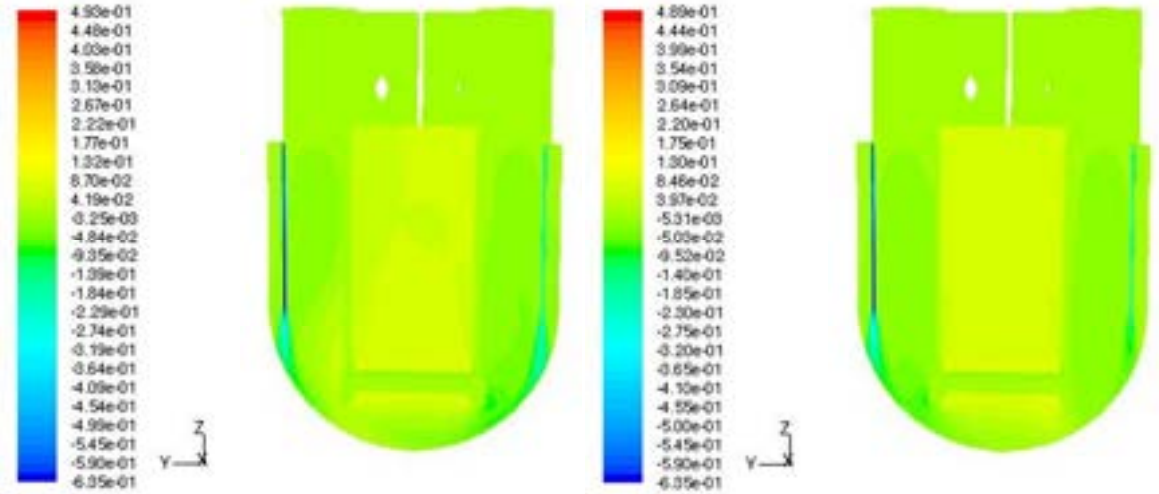

Figure 3.30. *z*-velocity distribution for the IRIS domain
(*t* = 60000 s, with supports, with gravity (left) and without gravity (right)).

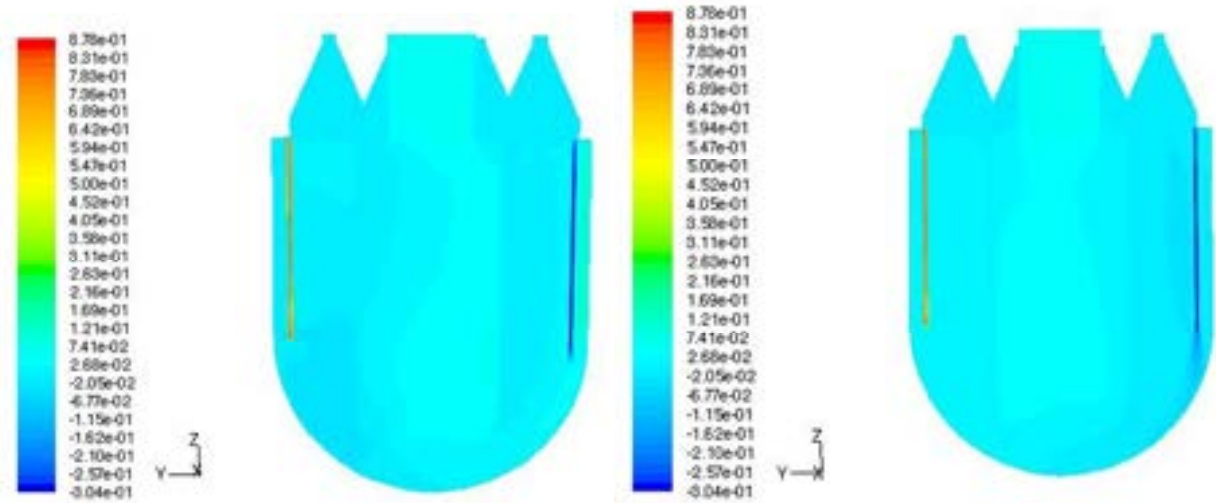

Figure 3.31. *z*-velocity distribution for the facility domain
(*t* = 600 s, constant residence time approach, with gravity (left) and without gravity (right)).

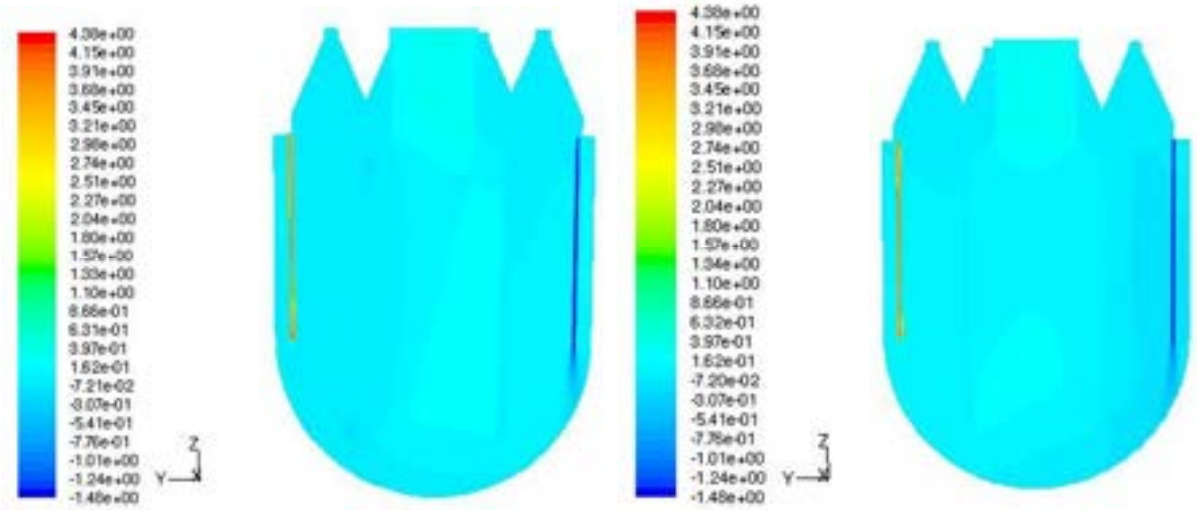

Figure 3.32. *z*-velocity distribution for the facility domain
(*t* = 600 s, constant velocity approach, with gravity (left) and without gravity (right)).

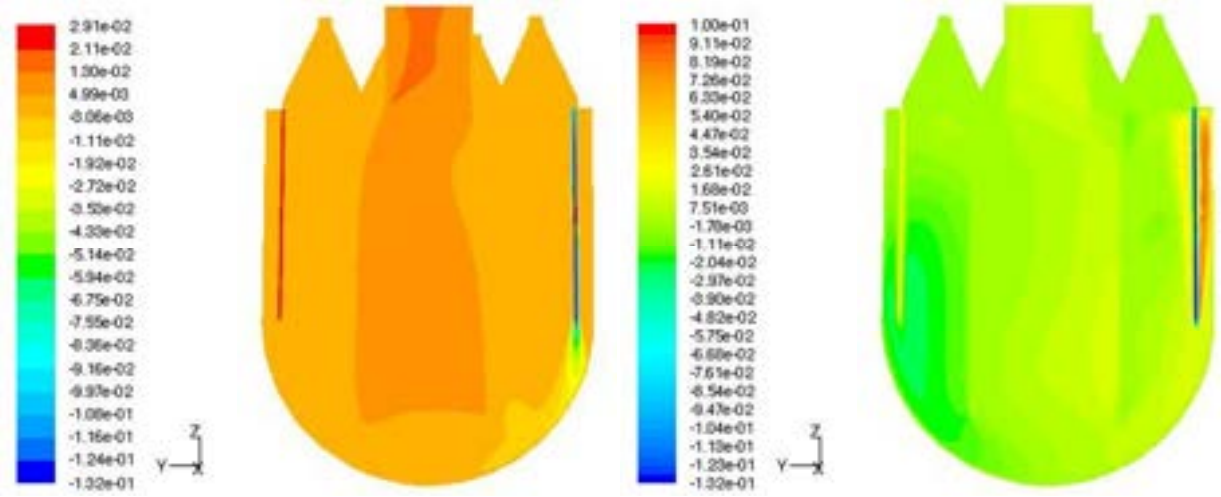

Figure 3.33. *z*-velocity distribution for the facility domain
(*t* = 20000 s, constant residence time approach, with gravity (left) and without gravity (right)).

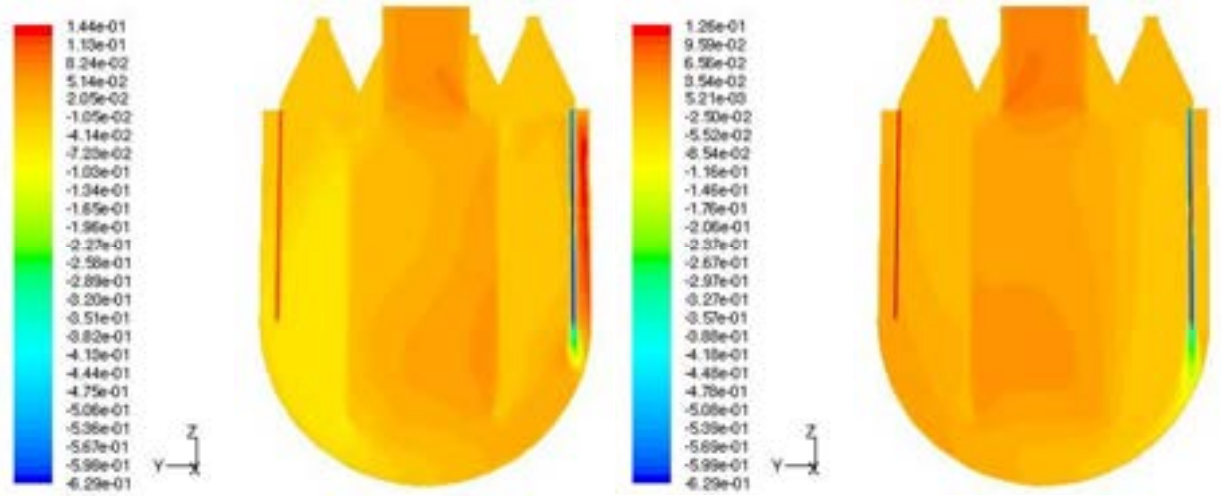

Figure 3.34 *z*-velocity distribution for the facility domain
(*t* = 20000 s, constant velocity approach, with gravity (left) and without gravity (right)).

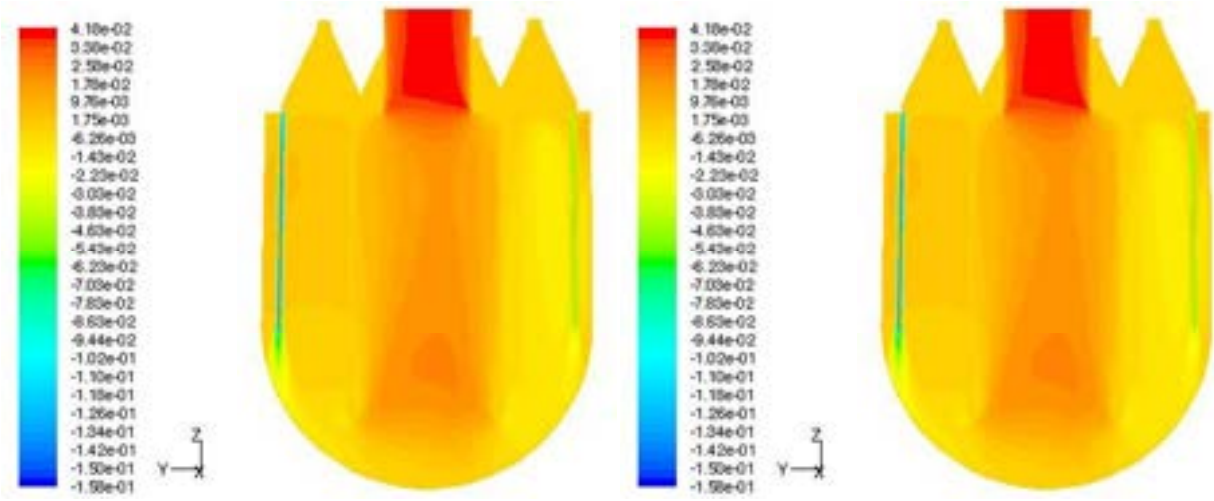

Figure 3.35 *z*-velocity distribution for the facility domain
(*t* = 60000 s, constant residence time approach, with gravity (left) and without gravity (right)).

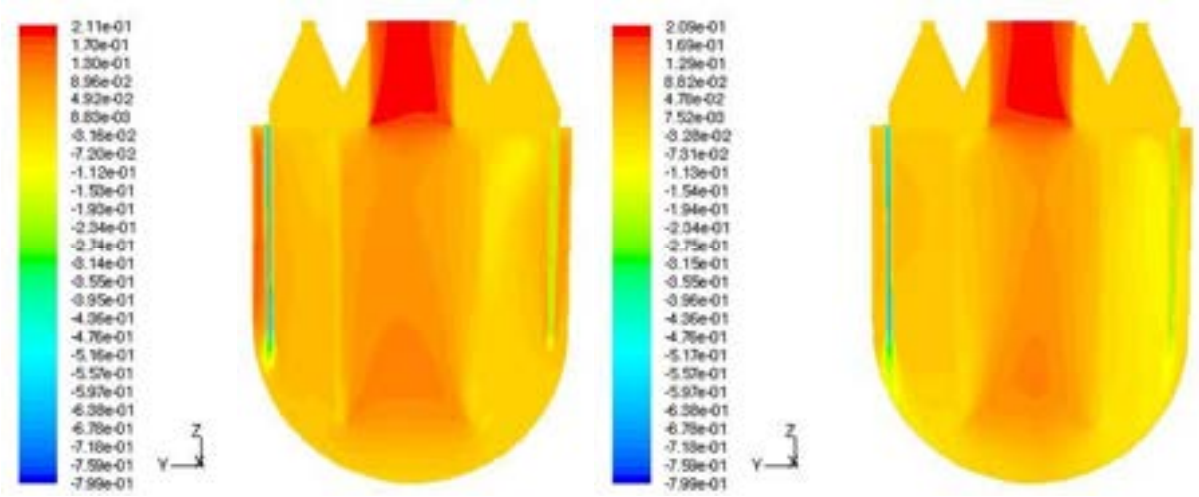

Figure 3.36. *z*-velocity distribution for the facility domain
(*t* = 60000 s, constant velocity approach, with gravity (left) and without gravity (right)).

Concerning the IRIS simulations, the mass flow rates in the downcomer keep a similar distribution both in the case with gravity and in the case without gravity: even if different fluids having different temperatures are injected by the SGs and the DVI lines, the presence of the gravity field does not affect strongly their behaviour and their distribution. This is also shown in fig. 3.37, in which the velocity vector distribution in the lower part of IRIS is plotted for the time window *t* = 20000 s after the line break. For this time window we observe the smallest mass flow rates from the DVIs (as reported in tab. 1.2) and so it represents the most critical case among that simulated to have a reverse flow back in the DVI pipe: as we can see from the vector distribution, the flow rate maintains the expected behaviour as in the previous cases without gravity.

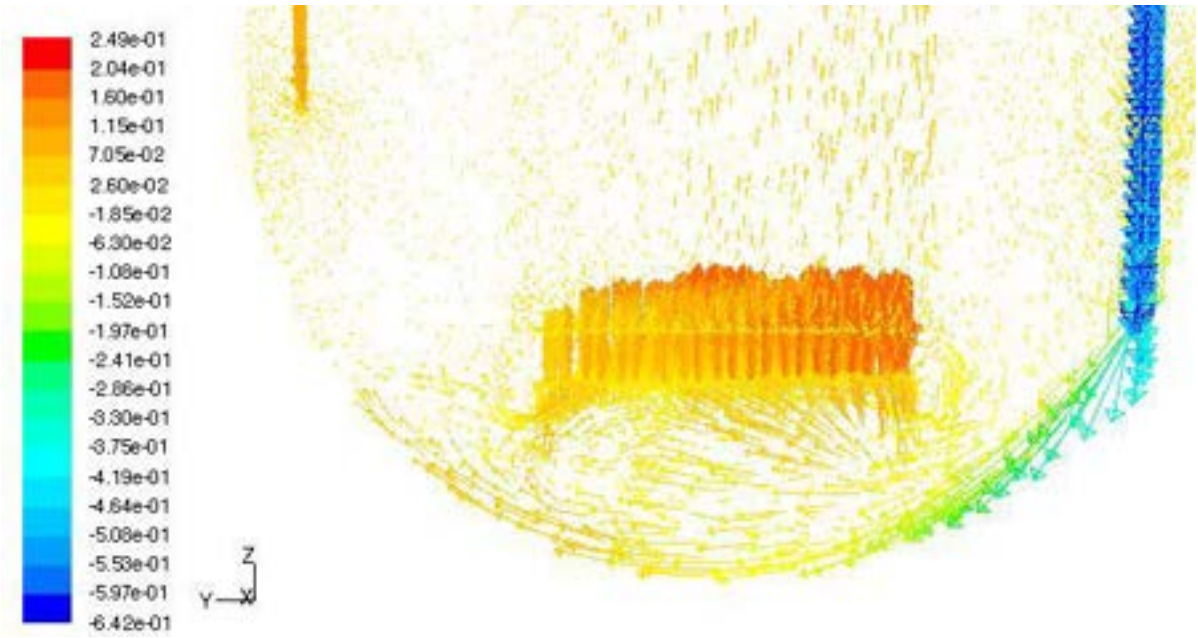

Figure 3.37. Velocity vector distribution, coloured for *z*-velocity, in the lower part of IRIS (t = 20000 s, with supports and with gravity).

The same observations cannot be made for the facility. Due to the low mass flow rates considered and due to the assumption of adopting a cooler temperature for the water injected from the SGs to the downcomer than that injected through the DVI lines, positive values of the *z*-velocity are observed in the zones close to the intact DVI line, as plotted in fig. 3.38.

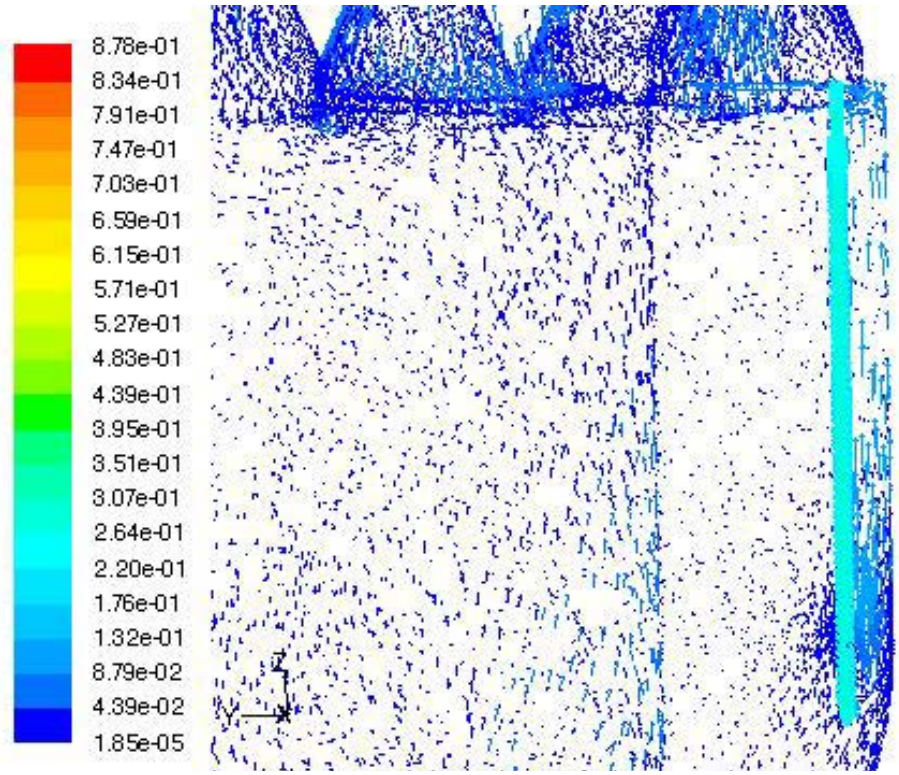

Figure 3.38. Velocity vector distribution, coloured for *z*-velocity, for the facility in the region close to intact DVI line (t = 600 s, with gravity, constant residence time approach).

It can be concluded that assuming a hotter water injection through the DVI lines is a too strong option which will not allow to perform correct experiments on the facility, since it is noted from the simulations performed under a gravity field that a large part of the water coming from the DVI will rise up back to the DVI channel immediately after the injection.

It has been investigated also the possibility to change the temperature of the water injected by the SGs and the DVI lines, and its effect on the computational simulations. In order to study this possibility, a new simulation has been performed by considering the temperature of the mass flow rate from the intact DVI line at T = 293.15 K and the temperature value of the mass flow entering from the SGs set equal to T = 343.15 K.

It has been simulated only one case, i.e. t = 20000 s after the DVI line break, by considering the velocity constant scaling approach. The results are shown in fig. 3.39.

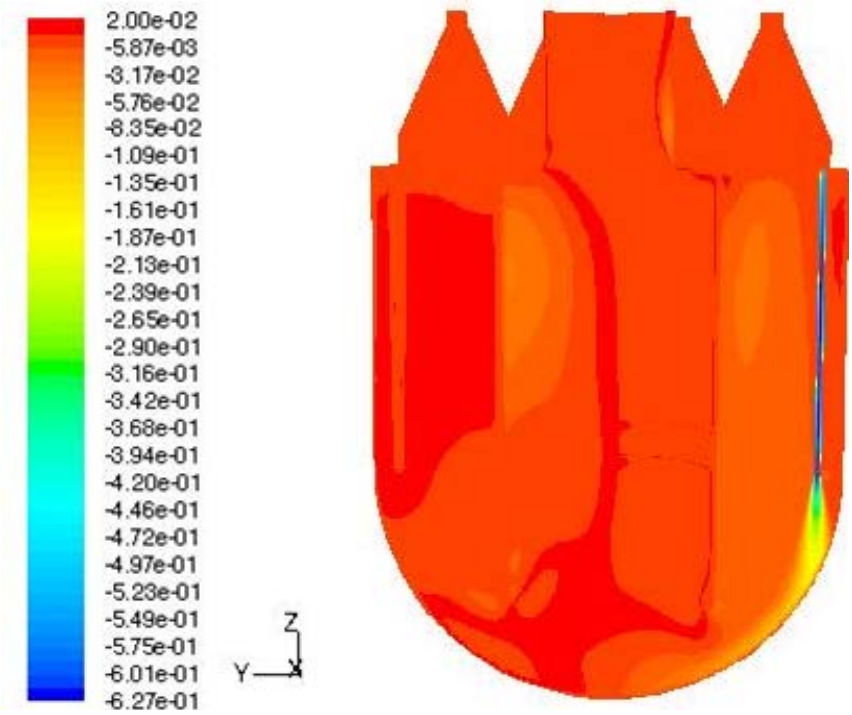

Figure 3.39. z-velocity distribution for the facility domain,
by imposing T_{SG} = 343 K and T_{DVI} = 293 K
(t = 20000 s, constant velocity scaling approach, with gravity).

We can see that even if gravity is considered, changing temperatures is enough to avoid the possibility of rising fluxes to the DVI pipe due to different density values. For completeness, also the temperature field is reported, for the same case, by neglecting gravity, in fig. 3.40 and in fig. 3.41.

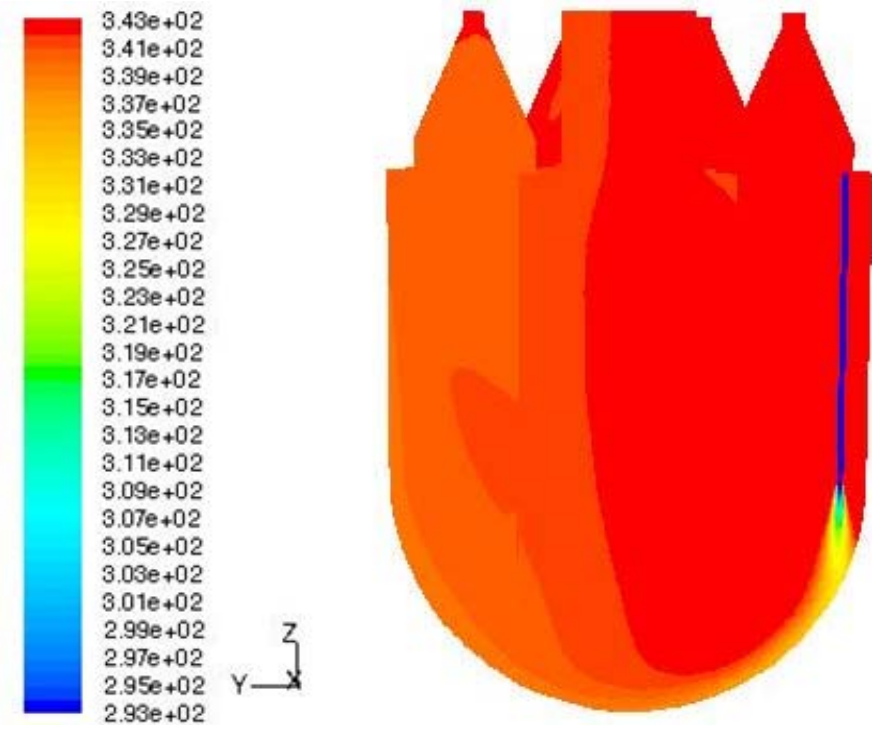

Figure 3.40. Temperature distribution for the facility domain,
by imposing T_{SG} = 343 K and T_{DVI} = 293 K,
(t = 20000 s, constant velocity scaling approach, without gravity).

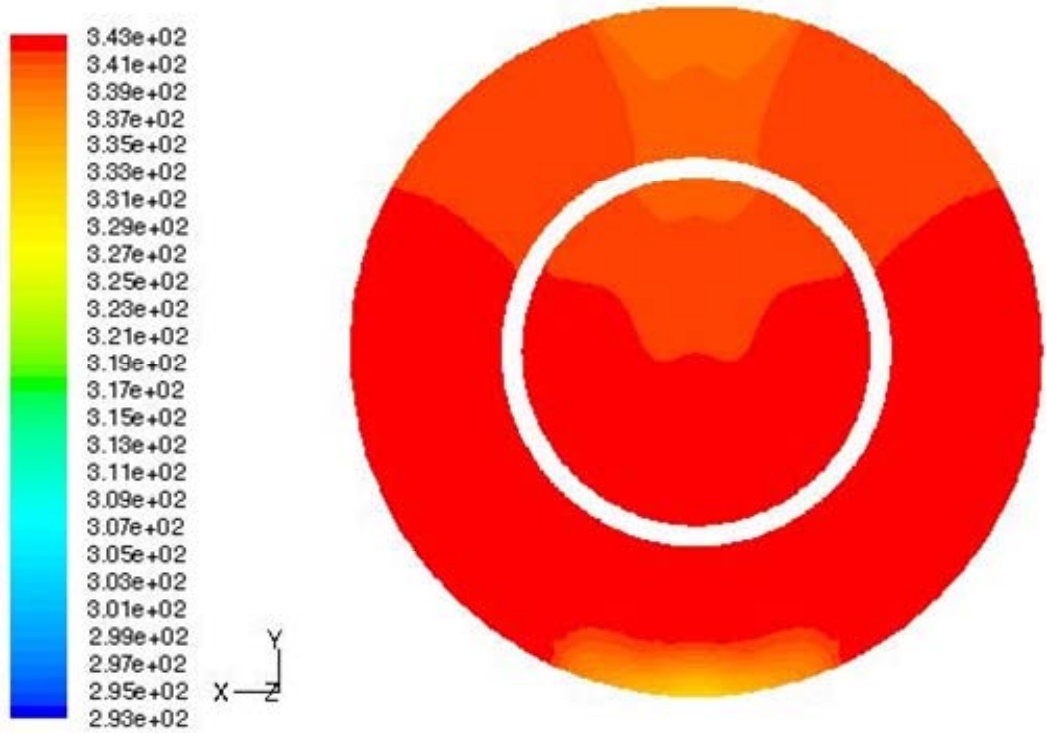

Figure 3.41. Facility temperature distribution at the core inlet section,
by imposing T_{SG} = 343 K and T_{DVI} = 293 K
(t = 20000 s, constant velocity scaling approach, without gravity).

3.3 DVI length influence on the temperature field

The goal of this analysis is to study the effects of different DVI lengths on the temperature field and on the mixing processes in the IRIS downcomer. Four different DVI lengths have been considered (as reported in fig. 3.42 and in fig. 3.43). Contours of temperature for all these cases are shown from fig. 3.44 to fig. 3.47, both with and without the gravity field, in order to observe the differences between each choice and to have an idea of which solution should be better to get a less sharp and smoother temperature distribution (i.e. boron concentration) at the core inlet. Furthermore, the results are analysed both for the global IRIS view and for the section referred to the core inlet. For the simulations it has been considered the IRIS model with core supports. The time window considered is t = 600 s after the DVI line break.

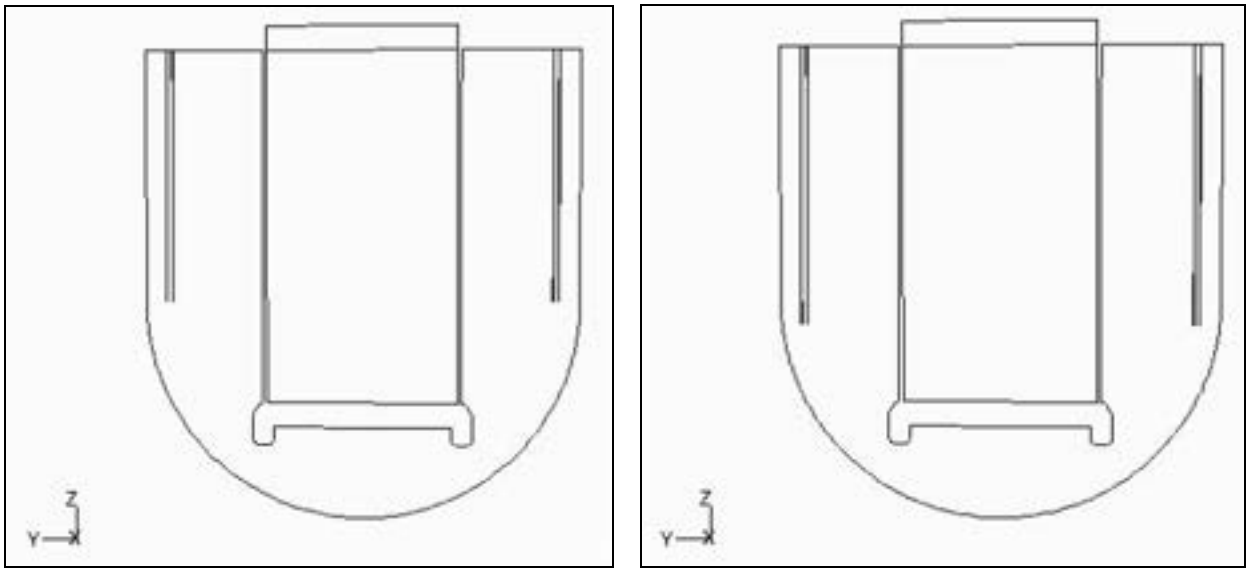

Figure 3.42. IRIS DVIs different length: nominal DVI length (left)
and a DVI line 0.3587 m longer than the nominal (right).

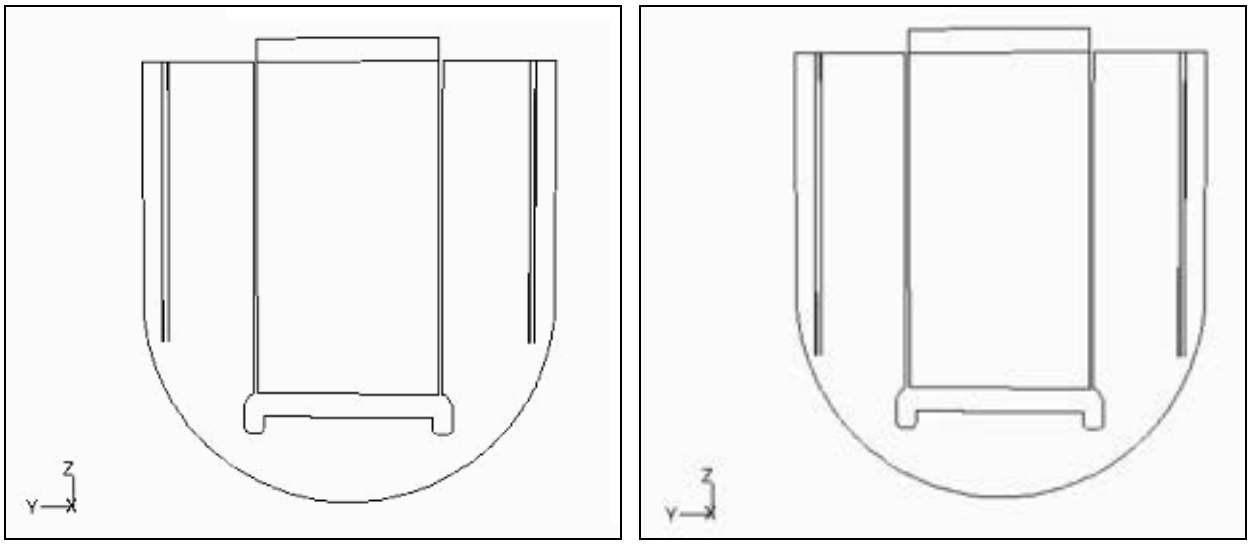

Figure 3.43. IRIS DVIs different length: a DVI line 0.6583m longer than the nominal (left) and a DVI line 0.9583 m longer than the nominal (right).

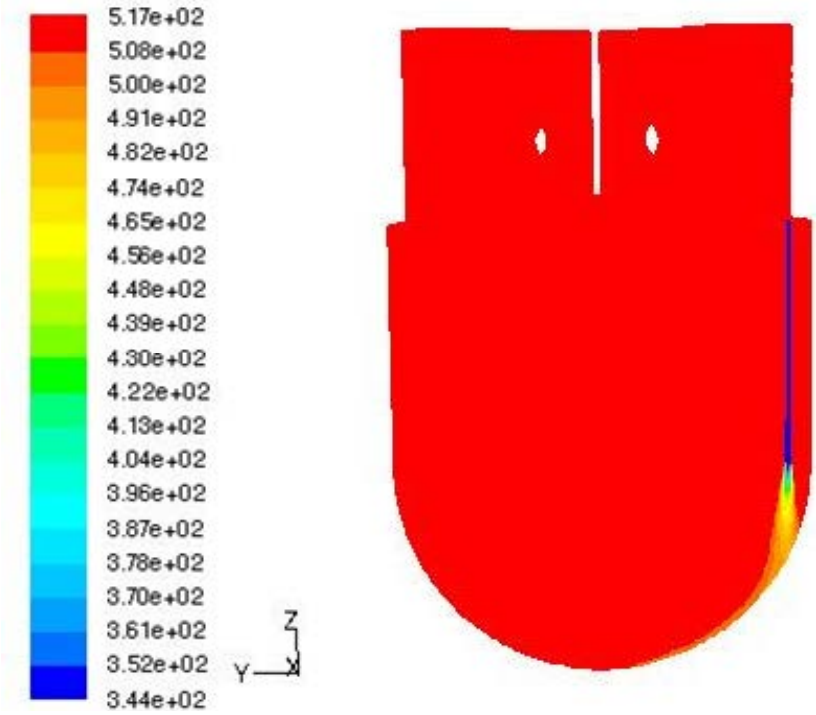

Figure 3.44. Temperature field for the IRIS domain
(t = 600 s, DVI of nominal length, with gravity, with supports).

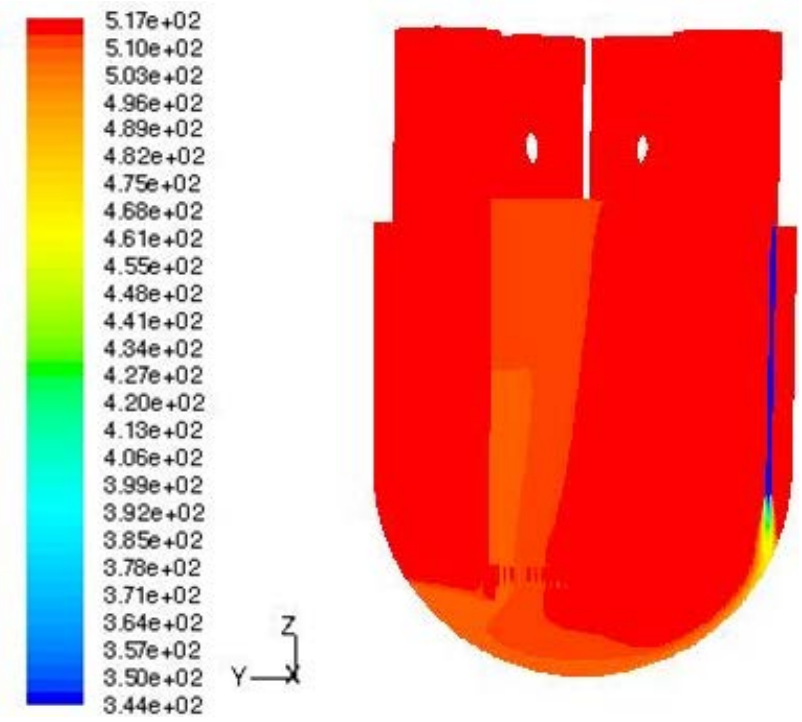

Figure 3.45. Temperature field for the IRIS domain
(*t* = 600 s, DVI 0.3583 m longer than the nominal length, with gravity, with supports).

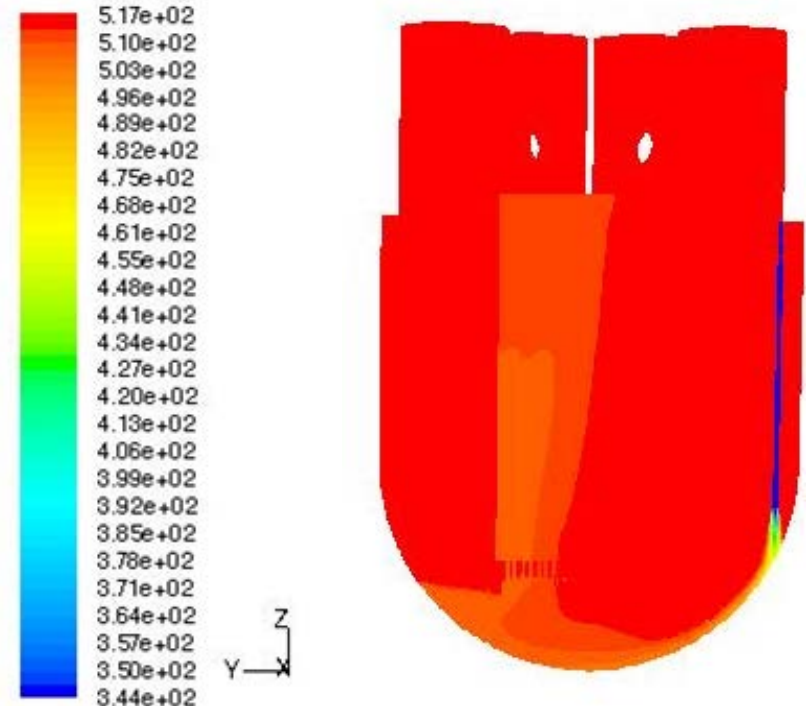

Figure 3.46. Temperature field for the IRIS domain
(*t* = 600 s, DVI 0.6583 m longer than the nominal length, with gravity, with supports).

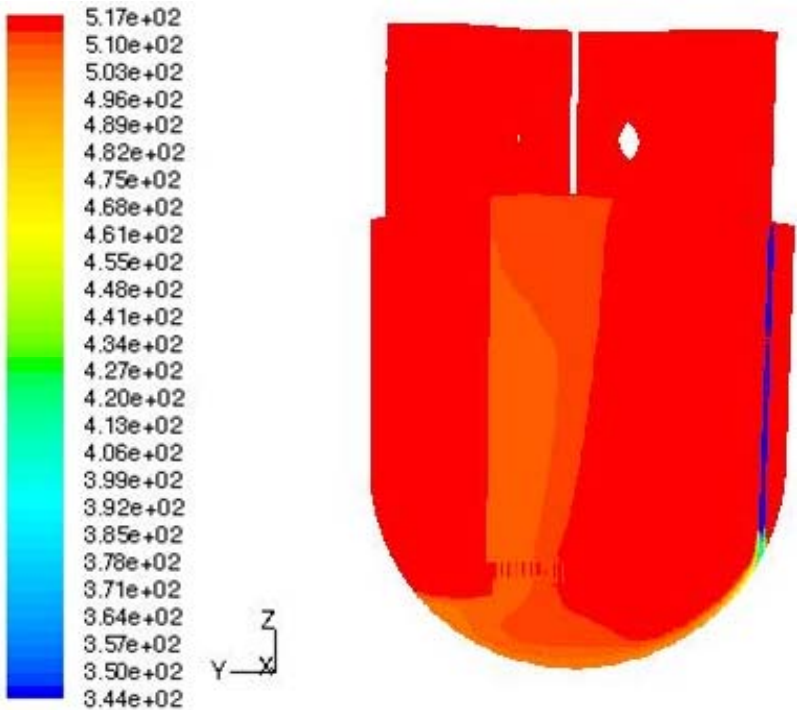

Figure 3.47. Temperature field for the IRIS domain
(t = 600 s, DVI 0.9583 m longer than the nominal length, with gravity, with supports).

Analysing the temperature field, when the gravity field is considered and when the DVI line length is nominal (i.e. of the same length of that provided for the IRIS reactor), the mixing processes seem to be less important compared to the cases when the DVI length is increased. A deeper analysis shows that some mixing phenomena are present, as shown in fig. 3.48, where the velocity field is reported.

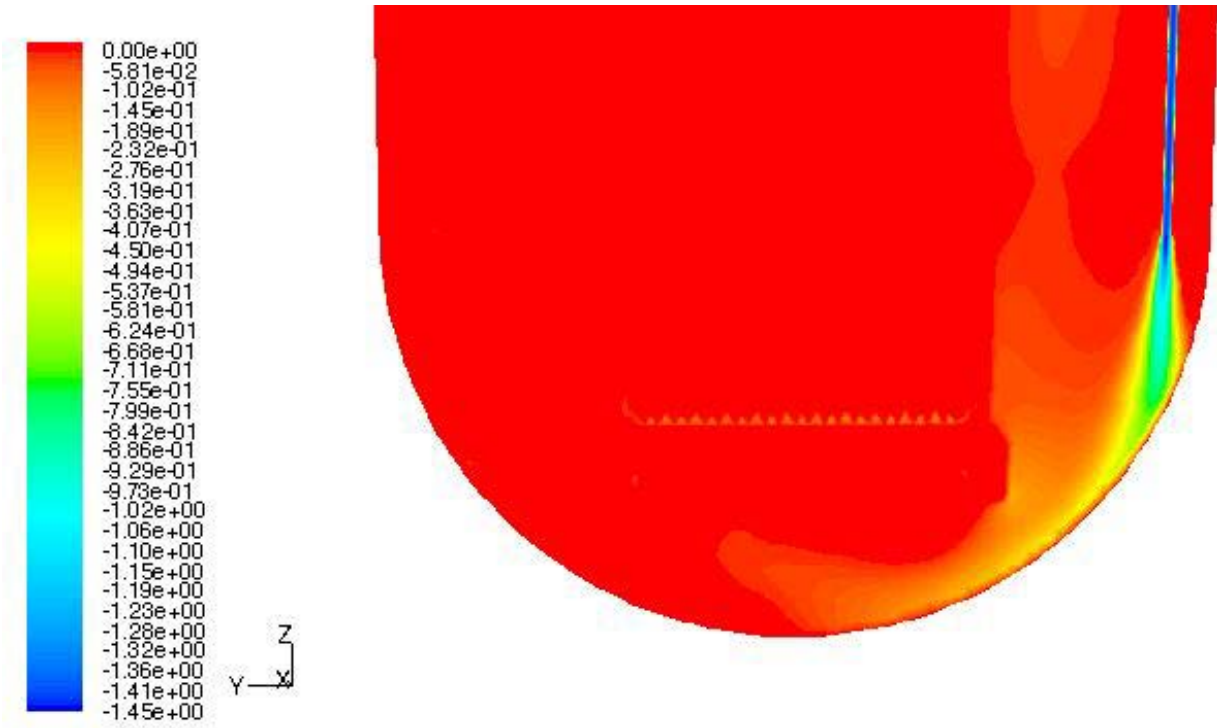

Figure 3.48. *z*-velocity distribution for the IRIS domain
(*t* = 600 s, DVI of nominal length, with gravity).

The mass flow rate coming from the intact DVI line and entering in the inlet core section covers a smaller area increasing the DVI length, as it is shown from fig. 3.49 and from fig. 3.50.

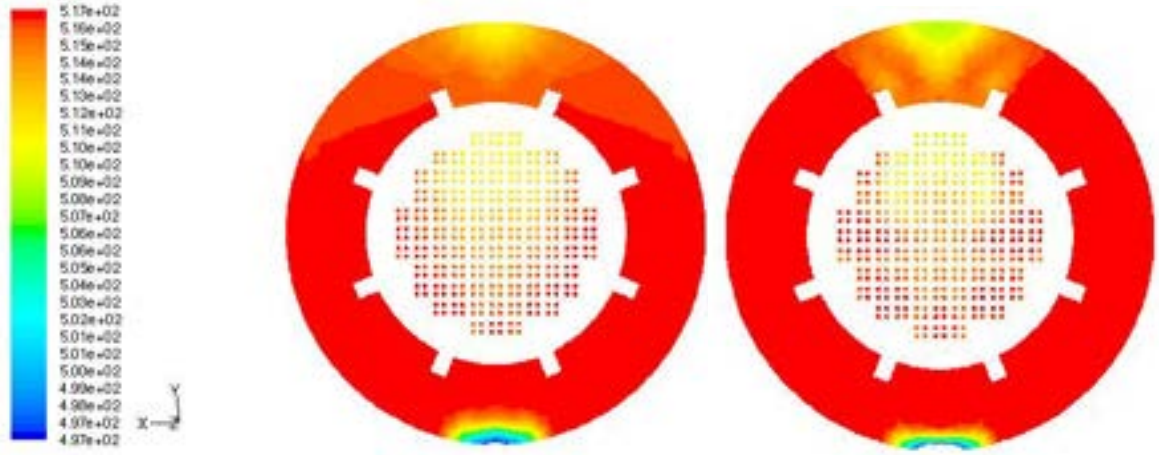

Figure 3.49. Temperature distribution at the core inlet section for the IRIS domain
(*t* = 600 s, with supports, with gravity, DVI of nominal length (left) and DVI 0.3586 m longer than the nominal length (right)).

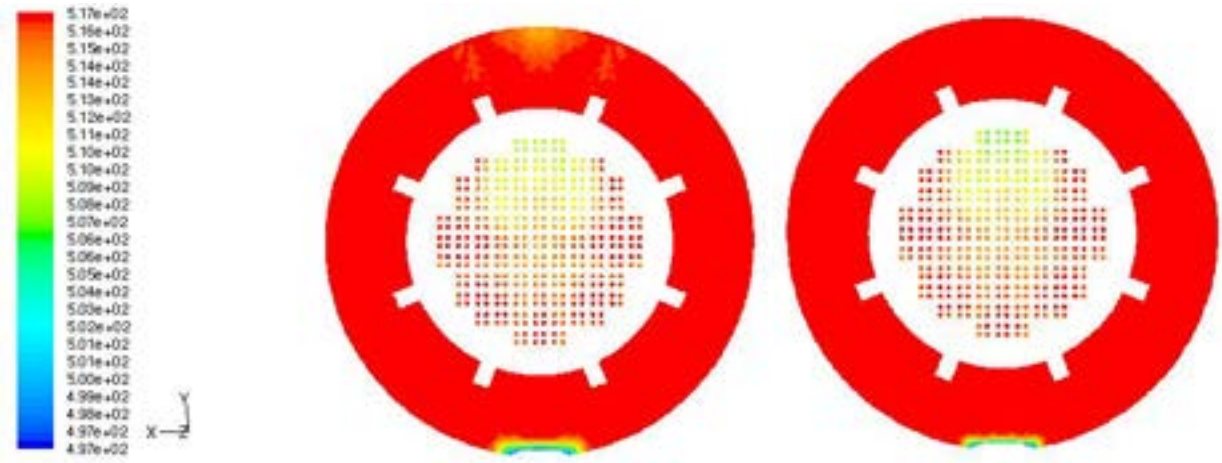

Figure 3.50. Temperature distribution at the core inlet section for the IRIS domain (t = 600 s, with supports, with gravity, DVI 0.6586 longer than the nominal length (left) and DVI 0.9586 m longer than the nominal length (right)).

In order to get a qualitative value of the mixing processes in the downcomer between the mass flow rates from the steam generators and from the DVI lines, the same simulations shown above have been repeated neglecting the gravity field, as reported in fig. 3.51 and fig. 3.52.

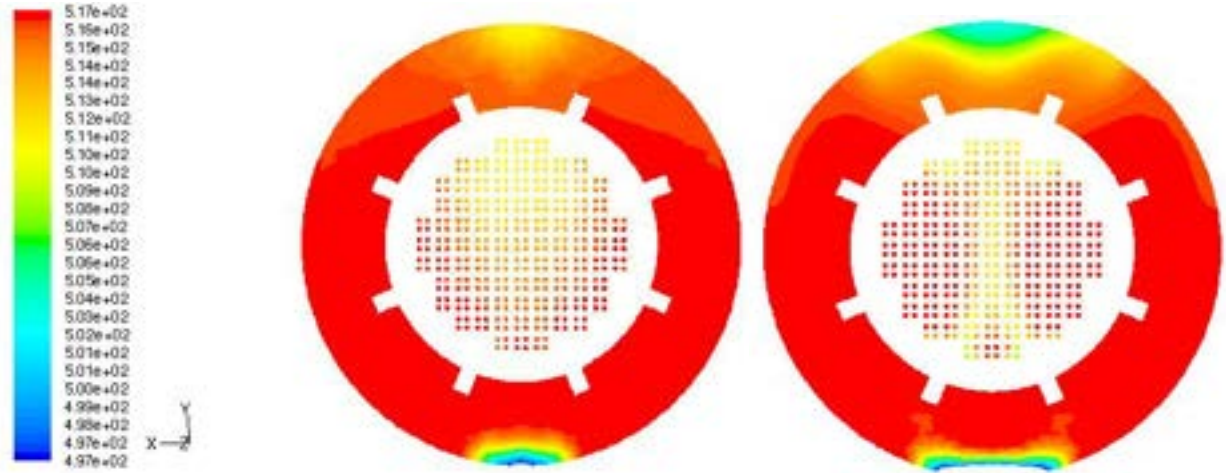

Figure 3.51. Temperature distribution at the core inlet section for the IRIS domain (t = 600 s, with supports, without gravity, DVI of nominal length (left) and DVI 0.3586 m longer than the nominal length (right)).

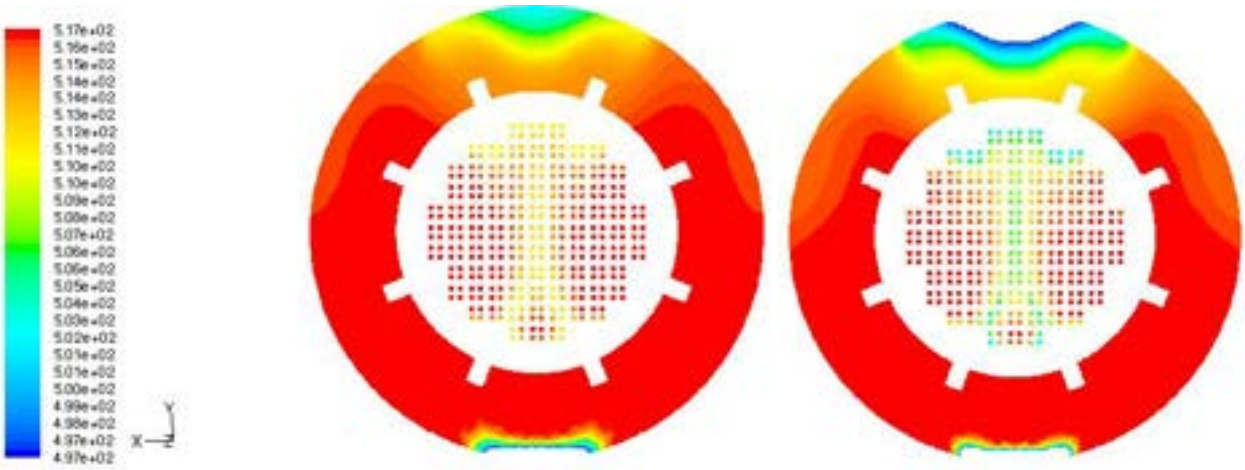

Figure 3.52. Temperature distribution at the core inlet section for the IRIS domain (t = 600 s, with supports, without gravity, DVI 0.6586 longer than the nominal length (left) and DVI 0.9586 m longer than the nominal length (right)).

As it can be seen in figures 3.51 and 3.52, when the DVI length increases, the temperature values in some holes of the perforated plate increase, even if the number of holes involved in the mixing process decreases. Observing the average are weighted temperature, evaluated considering only the free surface of the perforated plate, it can be noted that the average value of temperature does not change so much if the DVI length changes, even if the temperature distribution at the core inlet section is largely affects by the changing the DVI length. In tab. 3.2 the average area weighted temperature for each DVI length simulated are reported (both with gravity field and without gravity field).

DVI length [m]	**Average area weighted Temperature [K]**
	With gravity
Nominal	514.64
Nominal + 0.3586 m	514.78
Nominal + 0.6586 m	514.73
Nominal + 0.9586 m	514.70
	Without gravity
Nominal	515.15
Nominal + 0.3586 m	515.22
Nominal + 0.6586 m	515.16
Nominal + 0.9586 m	515.20

Table 3.2. Average temperature values at the IRIS core inlet for different DVI lengths (t = 600 s, with core supports, with and without gravity).

CONCLUSIONS

Computational results have been obtained with the CFD FLUENT code for both the models of IRIS and of the facility in construction at the DIMNP of the University of Pisa. The preliminary results concern the facility computational model: it has been considered the adoption of a porous region in each of the SGs to obtain velocity profiles uniform and normal to the inlet sections. If those regions are not considered, a non homogeneous distribution of the velocity in the z coordinate is achieved, and this should affects the velocity profile in the whole facility. These results suggest the adoption of grids to be placed at the eight inlet sections of the facility in construction.

The simulations have been performed considering three temporal windows (t = 600 s, t = 20000 s and t = 60000 s) after a DVI line break accident. Concerning the temperature field (i.e. boron concentration) it has been observed the importance of the core supports on the IRIS fluid-dynamics. When they have been considered in the modelling, the temperature profile obtained at the IRIS core inlet was smoother, i.e. the cold mass flow rate coming from the intact DVI influenced the core inlet zone much more: the flow rate from the DVI impact the supports and it is deviated, covering a larger part of the core inlet. The temperature field obtained at the core inlet section of IRIS and of the facility have been investigated deeply in order to figure out if the experimental facility could effectively reproduce the mixing processes expected in the reactor during a SBLOCA; from the performed simulations it has been noted that the temperature distribution in IRIS is in general very similar to that observed in the facility. The average temperature profiles obtained in IRIS and in the facility are quite close to each other for the three time windows considered after the DVI line break accident.

In particular, a better agreement between the results obtained for IRIS and for the facility is achieved using the constant velocity scaling approach to scale the flow rates entering to the facility. On the contrary, if the residence time scaling approach is adopted, lower flow rates are observed and the mixing processes in the downcomer are less important.

When the temperature of the DVI mass flow rate coming in the facility is higher than the temperature of the mass flow rate entering through the steam generators, an important part of the water flux from the DVI starts rising immediately at the injection due to the buoyancy, and this could cause distortions with respect to the IRIS behaviour. By the way, it has been tested in one case that the rising effect is greatly reduced if the

temperature of the mass flow entering from the SGs is kept at a higher value than that of the mass flow rate entering from the DVI lines (as it happens in IRIS), but this choice, at the same time, can create experimental problems due to the greater water flow rate that must be heated.

Moreover, it has been noted that the DVI length has a wide influence on the temperature field at the core inlet section of IRIS. If the DVI length increases, even if the average temperature value does not change, a completely different temperature profile is observed at the reactor core inlet. In particular, if the DVI length increases, a smaller part of the core inlet section will be affected by a higher temperature value, while the remaining part of the core inlet will keep a temperature value similar to that of the mass flow coming from the SGs.

REFERENCES

[1] W. Ambrosini, N. Forgione, F. Oriolo, “Analyses in Support to IRIS Reactor Vessel Downcomer and Lower Plenum Flow Test”, 18° IRIS Team Meeting, Tirrenia, October 9-12, 2007.

[2] M. E. Pasquini, “Analisi dei fenomeni di miscelamento nel downcomer e nel lower plenum del reattore IRIS mediante il codice STAR-CCM+”, DCMN UNIPI, Pisa, 2009.

[3] W. Ambrosini, N. Forgione, A. Frisani, A. Manfredini, F. Oriolo, “IRIS Reactor Vessel Downcomer and Lower Plenum Flow Test Scaling Approach”, DCMN UNIPI,Pisa, January 2006.

[4] F. Martiello, “Boron mixing issue in Downcomer and Lower Plenum of IRIS reactor”, RELAP simulated DVI-SBLOCA and Steam Line Break Accident, transient analysis and relevant data for boron mixing issue, DCMN UNIPI, Pisa, 2008.

[5] W. Ambrosini, A. Manfredini, F. Martiello, F. Oriolo, G. Simonini, N. Forgione, “Mixing phenomena in the IRIS reactor vessel: analysis of phenomena and preliminary design of a facility”, CIRTEN CERSE - UniPi RL – 1074/2009, Pisa March 2009.

[6] M. Turrin, “Mixing phenomena in the IRIS reactor vessel: preliminary design of a facility and arrangement of measurements”, Pisa December 2009.

[7] W. Ambrosini, N. Forgione, A. Manfredini, F. Oriolo, M.E. Pasquini, “CFD analysis of mixing phenomena in the IRIS reactor vessel downcomer and lower plenum”, The 13th International Topical Meeting on Nuclear Reactor Thermal Hydraulics (NURETH-13), Kanazawa City, Ishikawa Prefecture, Japan, September 27 – October 2, 2009.